NATIONAL ADVISORY COMMITTEE FOR AERONAUTICS

REPORT No. 750

HIGH-SPEED TESTS OF A MODEL TWIN-ENGINE LOW-WING TRANSPORT AIRPLANE

By JOHN V. BECKER and LLOYD H. LEONARD

1942

AERONAUTIC SYMBOLS

1. FUNDAMENTAL AND DERIVED UNITS

	Symbol	Metric		English	
		Unit	Abbreviation	Unit	Abbreviation
Length	l	meter	m	foot (or mile)	ft (or mi)
Time	t	second	s	second (or hour)	sec (or hr)
Force	F	weight of 1 kilogram	kg	weight of 1 pound	lb
Power	P	horsepower (metric)		horsepower	hp
Speed	V	kilometers per hour	kph	miles per hour	mph
		meters per second	mps	feet per second	fps

2. GENERAL SYMBOLS

W Weight$=mg$

g Standard acceleration of gravity$=9.80665$ m/s^2 or 32.1740 ft/sec^2

m Mass$=\frac{W}{g}$

I Moment of inertia$=mk^2$. (Indicate axis of radius of gyration k by proper subscript.)

μ Coefficient of viscosity

ν Kinematic viscosity

ρ Density (mass per unit volume)

Standard density of dry air, 0.12497 kg-m^{-4}-s^2 at 15° C and 760 mm; or 0.002378 lb-ft^{-4} sec^2

Specific weight of "standard" air, 1.2255 kg/m^3 or 0.07651 lb/cu ft

3. AERODYNAMIC SYMBOLS

S Area

S_w Area of wing

G Gap

b Span

c Chord

A Aspect ratio, $\frac{b^2}{S}$

V True air speed

q Dynamic pressure, $\frac{1}{2}\rho V^2$

L Lift, absolute coefficient $C_L=\frac{L}{qS}$

D Drag, absolute coefficient $C_D=\frac{D}{qS}$

D_0 Profile drag, absolute coefficient $C_{D0}=\frac{D_0}{qS}$

D_i Induced drag, absolute coefficient $C_{Di}=\frac{D_i}{qS}$

D_p Parasite drag, absolute coefficient $C_{Dp}=\frac{D_p}{qS}$

C Cross-wind force, absolute coefficient $C_C=\frac{C}{qS}$

i_w Angle of setting of wings (relative to thrust line)

i_t Angle of stabilizer setting (relative to thrust line)

Q Resultant moment

Ω Resultant angular velocity

R Reynolds number, $\rho\frac{Vl}{\mu}$ where l is a linear dimension (e.g., for an airfoil of 1.0 ft chord, 100 mph, standard pressure at 15° C, the corresponding Reynolds number is 935,400; or for an airfoil of 1.0 m chord, 100 mps, the corresponding Reynolds number is 6,865,000)

α Angle of attack

ϵ Angle of downwash

α_0 Angle of attack, infinite aspect ratio

α_i Angle of attack, induced

α_a Angle of attack, absolute (measured from zero-lift position)

γ Flight-path angle

REPORT No. 750

HIGH-SPEED TESTS OF A MODEL TWIN-ENGINE LOW-WING TRANSPORT AIRPLANE

By JOHN V. BECKER and LLOYD H. LEONARD

Langley Memorial Aeronautical Laboratory

Langley Field, Va.

NATIONAL ADVISORY COMMITTEE FOR AERONAUTICS

HEADQUARTERS, 1500 NEW HAMPSHIRE AVENUE NW., WASHINGTON, D. C.

Created by act of Congress approved March 3, 1915, for the supervision and direction of the scientific study of the problems of flight (U. S. Code, title 50, sec. 151). Its membership was increased to 15 by act approved March 2, 1929. The members are appointed by the President, and serve as such without compensation.

GEORGE W. LEWIS, *Director of Aeronautical Research* — JOHN F. VICTORY, *Secretary*

HENRY J. E. REID, *Engineer-in-Charge, Langley Memorial Aeronautical Laboratory, Langley Field, Va.*

SMITH J. DEFRANCE, *Engineer-in-Charge, Ames Aeronautical Laboratory, Moffett Field, Calif.*

EDWARD R. SHARP, *Administrative Officer, Aircraft Engine Research Laboratory, Cleveland Airport, Cleveland, Ohio*

TECHNICAL COMMITTEES

AERODYNAMICS
POWER PLANTS FOR AIRCRAFT
AIRCRAFT MATERIALS
AIRCRAFT STRUCTURES
INVENTION & DESIGNS
OPERATING PROBLEMS

Coordination of Research Needs of Military and Civil Aviation

Preparation of Research Programs

Allocation of Problems

Prevention of Duplication

Consideration of Inventions

LANGLEY MEMORIAL AERONAUTICAL LABORATORY

LANGLEY FIELD, VA.

AMES AERONAUTICAL LABORATORY

MOFFETT FIELD, CALIF.

AIRCRAFT ENGINE RESEARCH LABORATORY

CLEVELAND AIRPORT, CLEVELAND, OHIO

Conduct, under unified control, for all agencies, of scientific research on the fundamental problems of flight

OFFICE OF AERONAUTICAL INTELLIGENCE

WASHINGTON, D. C.

Collection, classification, compilation, and dissemination of scientific and technical information on aeronautics

REPORT No. 750

HIGH-SPEED TESTS OF A MODEL TWIN-ENGINE LOW-WING TRANSPORT AIRPLANE

By John V. Becker and Lloyd H. Leonard

SUMMARY

Force tests were made of a ⅛-scale model of a twin-engine low-wing transport airplane in the NACA 8-foot high-speed tunnel to investigate compressibility and interference effects at speeds up to 450 miles per hour. In addition to tests of the standard arrangement of the model, tests were made with several modifications designed to reduce the drag and to increase the critical speed.

The results show serious increases in drag at critical Mach numbers ranging from about 0.47 to 0.60 due to the occurrence of compressibility burbles on the standard radial-engine cowlings, on sections of the wing as a result of wing-nacelle interference, and on the semiretracted main landing wheels. The critical speed at which the shock occurred on the standard cowlings was 20 miles per hour lower in the presence of the fuselage than in the presence of only the wing. The drag of the complete model was reduced 25 percent at 300 miles per hour by completely retracting the landing gear, fairing the windshield irregularities, and substituting streamline nacelles (with allowance made for the proper amount of cooling-air flow) for the standard nacelle arrangement. The values of the critical Mach number were considerably increased as a result of the afore-mentioned improvements.

INTRODUCTION

The principal purpose of the reported tests was to investigate the effect of compressibility on the drag of the component parts of a representative large airplane and on the over-all drag of such an airplane. The influence of interference on compressibility effects was also to be studied. In addition, it was proposed to test several modifications of the standard component parts that gave promise of an improvement in aerodynamic characteristics.

The size of the NACA 8-foot high-speed tunnel made possible for the first time the testing of a complete ⅛-scale model at speeds up to 450 miles per hour. A widely used transport-type airplane was represented. The results of high-speed tests of various windshield arrangements on the same model have been presented in reference 1.

Previous high-speed tests in smaller wind tunnels have been concerned mainly with isolated bodies, particularly airfoils (references 2 and 3) and cylinders of fundamental shape (reference 4). A typical wing-nacelle combination with several cowling shapes was tested at high speeds in the investigation reported in reference 5. All these tests showed that, when the maximum local velocity near the surface of the body exceeded the local velocity of sound, a compression shock formed, resulting in a precipitous increase in drag coefficient with further increase in speed. The sea-level flight speed at which this phenomenon occurs may be as low as 300 miles per hour for a bluff body such as a sharp-edge radial-engine cowling (reference 5) or as high as 650 miles per hour for thin airfoils (reference 3), depending on whether the peak local velocity is much higher or only slightly higher than the flying speed. Reference 6 shows that the critical speed at which the shock occurs can be satisfactorily estimated from the peak local velocity on the body as computed from low-speed pressure measurements or from potential-flow theory.

The critical speeds of the various airplane component parts may be considerably lower in flight than the critical speeds indicated in tests of any one of the isolated parts because of mutual interference between the parts. Reference 6 suggests a method of estimating the effect of interference between two or more bodies from the measured or the theoretical pressure fields of the isolated bodies. The present tests provide a means of checking this method because critical speeds were obtained on several of the component parts alone and in combination.

The interference effect of the propeller slipstream on critical speeds is small at high flight speeds. In the present tests, which were made without propellers, the critical speeds of parts located in the slipstream may be reduced by the amount of the propeller slip.

The low turbulence level in the 8-foot high-speed tunnel (reference 7) permits extensive low-drag laminar boundary layers to be maintained on smooth models. Equally extensive laminar layers generally do not exist in flight on present-day aircraft owing to the effects of surface irregularities and high Reynolds numbers (references 8 and 9). Because the condition of the boundary layer has a large influence on the magnitude of the drag and the interference of the various airplane components, a special technique was employed during part of the present investigation to make the boundary

layers similar to those existing in flight. The locations of the transition from laminar to turbulent boundary layers were fixed near the leading edges of the various component parts by means of small-diameter thread doped to the surface. The results given in the tables and the figures reproduced with the main body of this report and labeled "with fixed transition" are thus quantitatively applicable to flight conditions, if the usual scale-effect corrections are made. In many cases, the results obtained on the smooth model and labeled "with natural transition" are given for comparative purposes. It has been found that, for this investigation, the results from the smooth models are suitable for qualitative comparisons. For example, the relative merit of various nacelle arrangements would be the same in flight as in the tests on the smooth model.

The critical speed at which the compressibility shock occurs is independent of the state of the boundary layer as long as the boundary-layer changes do not cause serious changes in the flow outside the boundary layer. All the results given in this report are therefore pertinent with regard to the indication of critical speed.

A detailed discussion of the effect on drag and interference of the location of boundary-layer transition is given in a short appendix to the report. Correction factors are presented by which all the nacelle-drag data obtained on the smooth model may be reduced to the "fixed transition" or estimated flight condition.

The tests were conducted at Langley Memorial Aeronautical Laboratory in 1938.

LIST OF SYMBOLS

V airspeed

q dynamic pressure $(1/2\rho V^2)$

a speed of sound in air, miles per hour $(33.5\sqrt{460+t})$

t air temperature, °F

M Mach number (V/a)

R Reynolds number $(V\bar{c}/\upsilon)$

$\bar{c}$ mean aerodynamic chord, 1.44 feet

υ kinematic viscosity

S area of partial-span model wing enclosed in tunnel, 12.05 square feet

S_W area of full-span model wing, 15.42 square feet

S_T area of model tail surfaces, 4.56 square feet

F maximum cross section (0.267 sq ft for a single nacelle; 0.964 sq ft for the fuselage)

C_{D_F} absolute drag coefficient based on maximum cross section of nacelle or fuselage

C_{D_W} absolute drag coefficient based on area S_W

C_{D_T} absolute drag coefficient based on area S_T

C_{L_S} absolute lift coefficient based on area S

C_{L_W} absolute lift coefficient based on area S_W $\left[\dfrac{\text{lift of model}+q(S_W-S)\ (C_{L_S}\text{ of wing alone})}{qS_W}\right]$

$M_{\bar{c}/4}$ pitching moment about quarter-chord point of mean aerodynamic chord

$C_{m_{\bar{c}/4}}=\dfrac{M_{\bar{c}/4}}{qS\bar{c}}$

α angle of attack referred to chord line of wing, degrees

α_n nacelle angle of attack referred to thrust axis, degrees

Q quantity of air flow through single cowling, cubic feet per second

Δp pressure drop across engine baffle plate, pounds per square foot

K conductance $\left(\dfrac{Q}{FV\sqrt{\Delta p/q}}\right)$

C_f coefficient of mean skin friction $\left(\dfrac{\text{mean skin friction per unit area}}{q}\right)$

APPARATUS

The NACA 8-foot high-speed tunnel in which the tests were carried out is a single-return, circular-section, closed-throat wind tunnel. The airspeed is continuously controllable from about 75 to more than 500 miles per hour. The turbulence of the air stream as indicated by transition measurements on airfoils is unusually low but somewhat greater than in free air.

The model employed in the tests is a ⅛-scale reproduction of a modern transport airplane, which was chosen for convenience as being representative of large present-day airplanes. The general arrangement and dimensions of the model and the several variations tested are shown in figure 1. Figure 2 shows the standard model installed in the wind tunnel. The setup was unusual in that the outer portions of the wing extended through the tunnel walls and served as the means of support for the model. The tip sections not reproduced represent about 22 percent of the total wing area. This system permits the model scale to be much larger than for the usual arrangement and still allows a valid comparison of the effects of the component parts. The relatively larger forces enable a more accurate determination of the effects of the various parts. The method of support minimizes tare forces and also precludes the possibility of compressibility interference between the strut supports and the model.

The model was so constructed as to permit removal of all component parts; the effects of each part could therefore be individually studied.

Wing.—The constant-chord center section of the model wing (figs. 1 and 3) is of NACA 2215 airfoil section. The tapered portions are decreased in thickness to the NACA 2212 section at a station 50.58 inches outboard the center line of the model. The wing profile was found to conform closely to the specified ordinates and the surface is aerodynamically smooth.

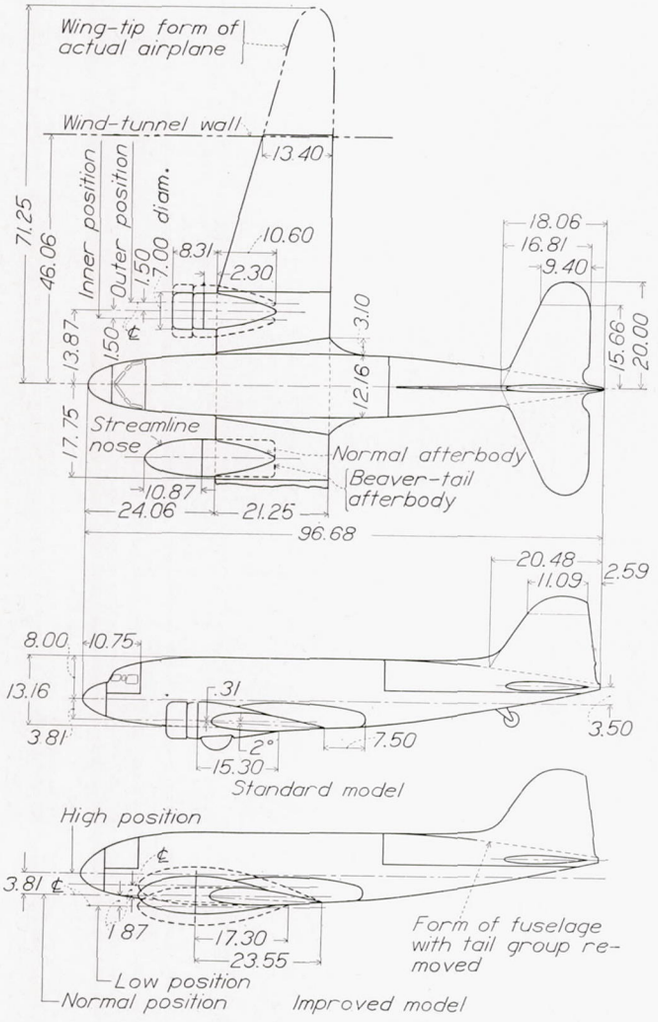

FIGURE 1.—General arrangement and dimensions (in.) of the standard model and the modifications tested.

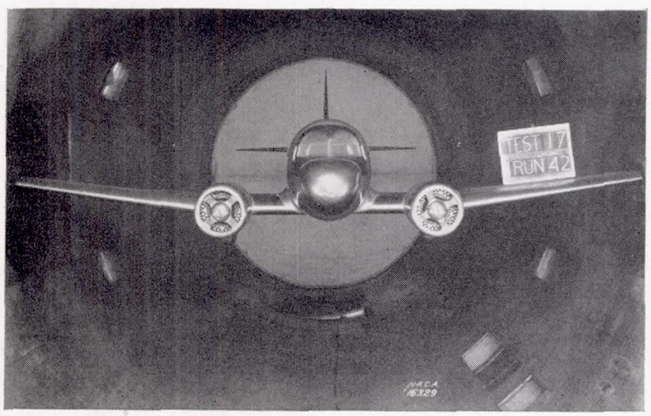

FIGURE 2.—Front view of the standard model mounted in the NACA 8-foot high-speed tunnel.

Fuselage, fillet, and tail group.—The fuselage details are shown in figures 1, 4, and 5. The nose sections and a section at the rear are removable so that alternate nose and tail arrangements can be tested. Before each series of tests, the fuselage surface was filled, spray-painted, and finished with fine sandpaper and polish.

The fillet was of the expanding type with increasing radius of curvature toward the rear.

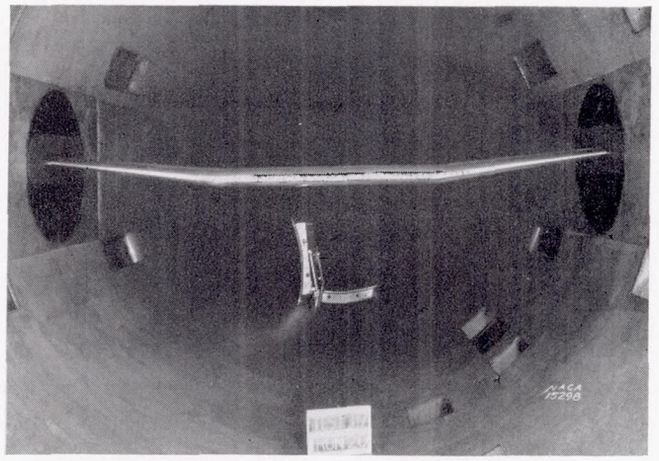

FIGURE 3.—Wing of transport model.

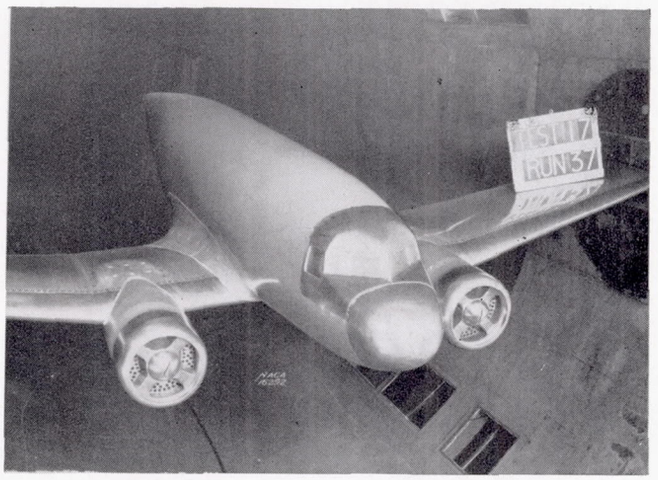

FIGURE 4.—Details of fuselage with standard windshield and fillet. Standard nacelles in low position.

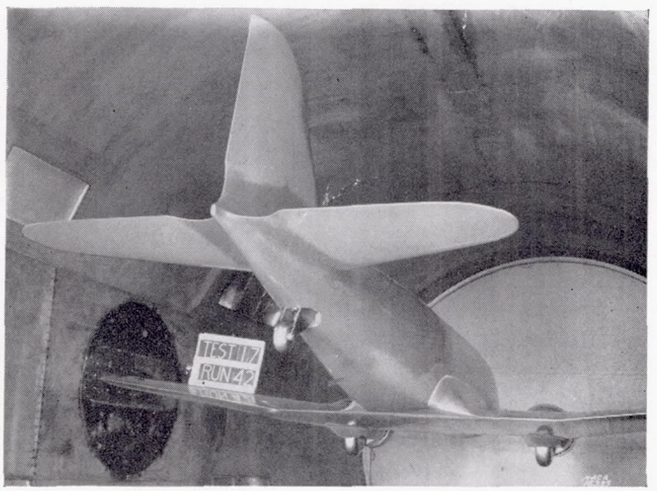

FIGURE 5.—Details of tail group, tail wheel, and fillet.

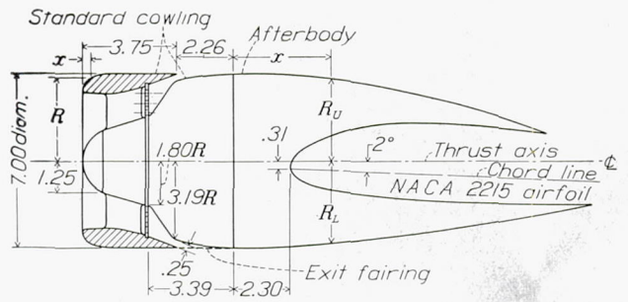

FIGURE 6.—Nacelle details. Standard cowling, normal position. Dimensions in inches.

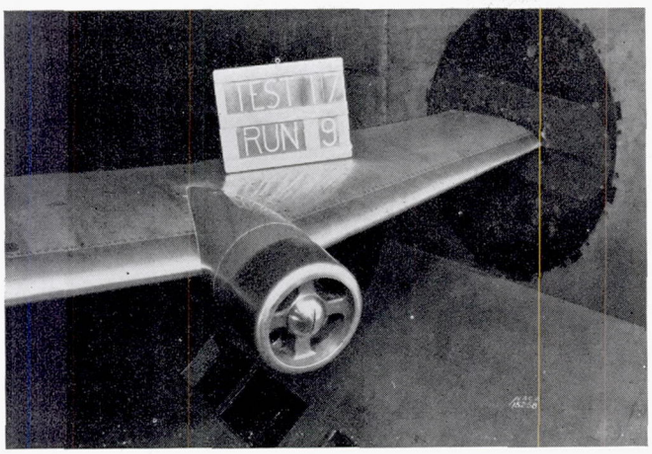

FIGURE 7.—Standard nacelle in normal position.

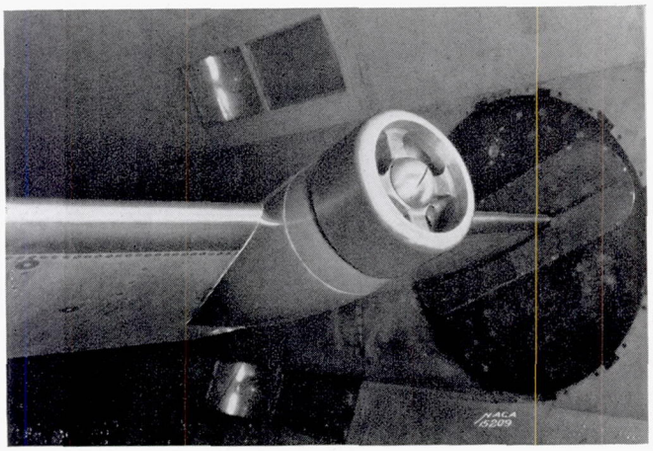

FIGURE 8.—Standard nacelle in low position.

The tail group is shown in figure 5. Unclassified symmetrical airfoil sections were used. The horizontal tail tapers in thickness from about 10 to 6 percent and the vertical surface from about 8 to 6 percent. The usual breaks in the surface at control-surface hinges are not represented.

Nacelles.—The nacelle shown in figure 6 is a ⅛-scale model of the normal 56-inch-diameter installation enclosing an 850-horsepower single-row radial engine. The exterior of the model nacelles is free of scoops, vents, and irregularities due to the landing gear. The wing has a chord of 21.25 inches and a thickness at the point of nacelle attachment of 3.19 inches. The fore-and-aft location of the nacelles was maintained constant in all the tests; the propeller plane was 42 percent of the chord ahead of the leading edge. The nacelle axes were inclined −2° with reference to the wing-chord line and were parallel to the fuselage reference line. The nacelles were tested in high and low positions for which the thrust axis was moved vertically 9 percent of the chord to make the nacelle tangent to the lower and the upper surfaces of the wing. For these positions, it was necessary to modify the fairing of the afterbody. Figures 1, 7, 8, and 9 show the fairing details for the three positions; table I gives the principal ordinates for the three afterbodies and for the standard cowling. Inner and outer positions of the nacelles were also tested; the nacelles in their normal vertical position were moved 21 percent of the nacelle diameter in a spanwise direction.

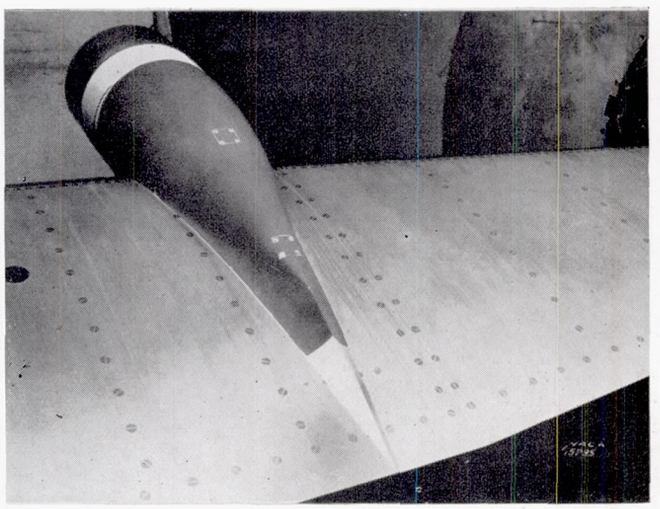

FIGURE 9.—Standard nacelle in high position. Exit slot covered.

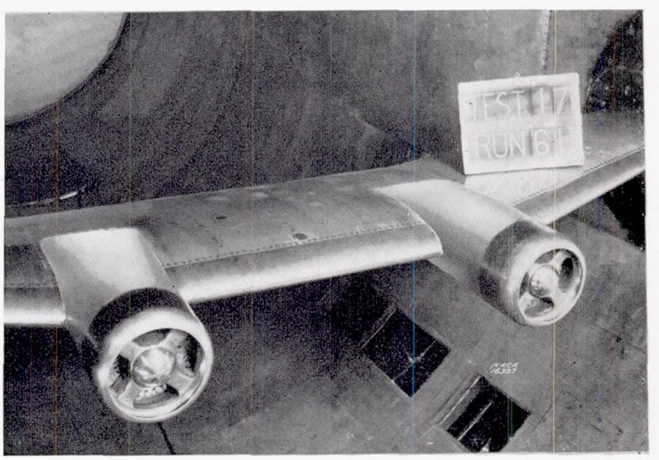

FIGURE 10.—Nacelles with beaver-tail afterbodies. Normal position. Exit slot covered.

A beaver-tail afterbody shape was tested with the nacelles in the normal position. This modification did not change the side-view profile but made the nacelles rectangular in plan view. (See figs. 1 and 10.)

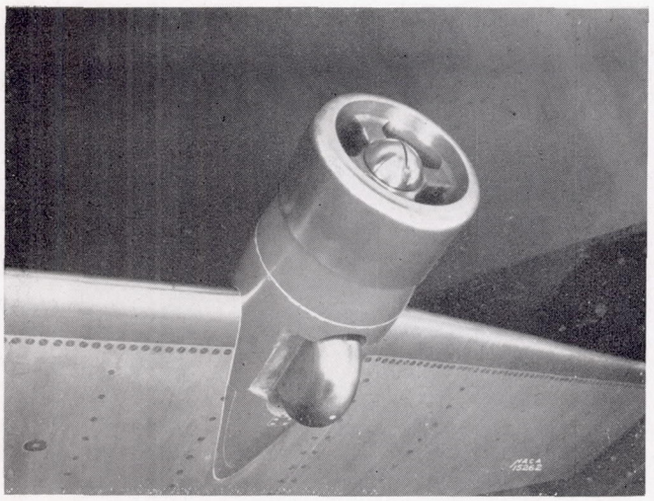

FIGURE 11.—Details of main wheels in retracted position. Nacelle in normal position.

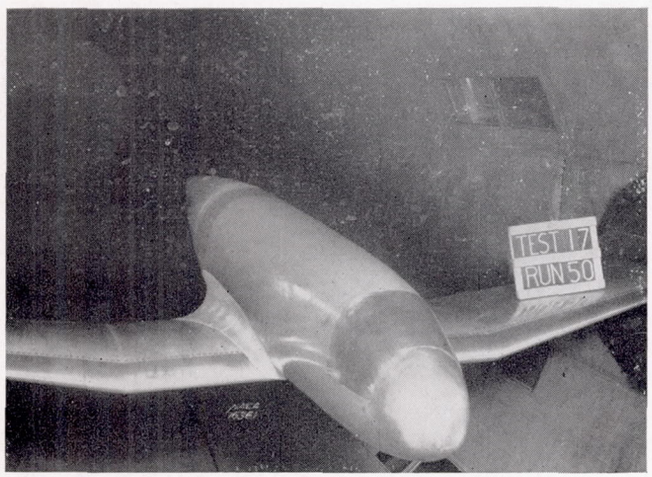

FIGURE 12.—Details of streamline nose replacing standard windshield.

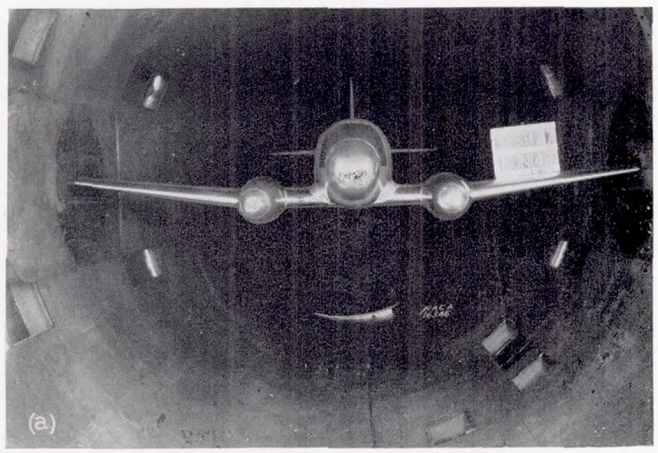

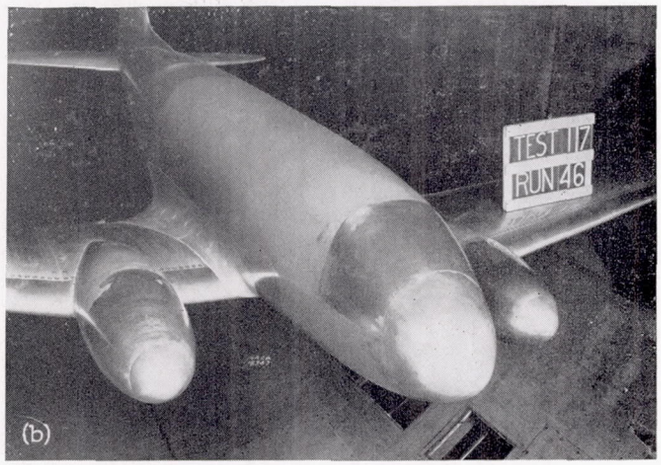

(a) Front view.
(b) Three-quarter view.

FIGURE 13.—Improved model.

Modifications to the standard cowling consisted in covering the exit slot between the cowling skirt and the inner cowling (figs. 6, 9, and 10) and the substitution of a streamline nose for the standard cowling. The streamline nose (fig. 1 and table I) was derived from NACA streamline form 111 (reference 10) for a fineness ratio of 4. The streamline nose was tested with the same afterbodies as the standard cowling. Combinations employing the streamline noses are hereinafter called streamline nacelles; and those employing the standard cowling are called standard nacelles, regardless of nacelle location.

The flow of air through the standard cowling was regulated by a baffle plate simulating the radial engine. The plate was perforated by one hundred ¼-inch holes, providing a conductance K of 0.08. The corresponding pressure drop $\Delta p/q$ across the baffle plate was computed by the method of reference 11 to be 0.80; and the flow quantity Q/FV, to be 0.072.

Additional tests with no air flow were made with all the holes closed, that is, with $K=0$, and also with alternate holes closed, for which $K=0.04$, $\Delta p/q=1.00$, and $Q/FV=0.04$.

On the model, as on the actual airplane, no provision is made for the control of cooling air by means of varying the width of the exit-slot opening. In all the tests with cooling-air flow, the width was 0.25 inch. In some of the tests without cooling air, the exit was covered, as has been described. No provision was made for cooling-air flow in the streamline nacelles.

Landing gear.—Details of the semiretracted landing gear are shown in figures 5 and 11. Unlike the full-scale installation, the inside of the wheel-well openings on the model was closed off from the interior of the nacelles.

Improved model.—The most effective modifications to the model were combined in what is called the improved model. The standard windshield and cockpit fairings were replaced by a streamline nose (figs. 1 and 12) in which the irregularity due to the windshield was completely faired out. The streamline nacelles were employed and the wheel and the wheel-well irregularities were completely removed. The improved model is shown in figure 13.

TESTS

The tests consisted in the measurement of lift, drag, and pitching moment at speeds ranging from 140 to 450 miles per hour. The tests could be carried beyond maximum lift at 140 miles per hour; but, at higher speeds, strength limitations determined the lift coefficient to which the tests could be extended. Thus, at 450 miles per hour, a lift coefficient of 0.2 was the greatest that could be obtained.

Tests were made of the wing alone and of the combinations necessary to obtain the following data:

1. Effective nacelle drag (without fuselage) with the various modifications to nacelle shape, nacelle location, and cooling-air flow. ("Effective drag" is herein defined as the difference in total drag measured with and without the part in question.)
2. Interference between nacelles and fuselage for all nacelle positions, with and without the tail group
3. Effective drag of fuselage and fillet with standard and faired windshield
4. Effective drag of tail group
5. Interference between tail group and nacelles
6. Effective drag of fillet and interference between fillet and tail group
7. Effective drag of semiretracted landing gear:
   (a) Main wheels
   (b) Tail wheel

For the most important configurations, tests were made both with natural transition and with transition fixed at 10 percent of the wing and the tail chords and near the noses of the streamline nacelles. A number of the tests of the nacelles were made only with smooth models.

RESULTS

The method of computing the airspeed, the Mach number, and the Reynolds number in the 8-foot high-speed tunnel is described in reference 12. According to standard practice, the true, rather than the indicated, dynamic pressure was used in computing coefficients from the force tests; the coefficients thus directly indicate any compressibility effects.

The greater part of the drag results is in the form of effective drag coefficients, which are herein defined as the difference in the total drag coefficients determined with and without the part in question. This difference in drag coefficient was computed at fixed angles of attack rather than at given lift coefficients, as is usually done in three-dimensional-flow setups. The choice of angle of attack as the independent variable was dictated by the fact that compressibility effects are governed primarily by the attitude of a body and not by the net lift of the body in combination with other shapes. Furthermore, the induced-drag changes due to small changes in lift are minimized in a setup such as the one employed in these tests, which was approximately two-dimensional. As a matter of fact, at subcritical speeds the effective drag as obtained at a given attitude was found to be almost exactly equal to that computed at a fixed lift coefficient.

With the model attitude fixed, compressibility effects are a function of Mach number, which is the flow-similarity index for compressible flow and has a significance similar to that of the Reynolds number in viscous flow. The results of these tests are accordingly plotted either as a function of Mach number for a particular attitude or as a function of angle of attack at a given Mach number.

If the air temperature is known, the airspeed, in miles per hour, corresponding to a given Mach number can be directly computed from the relation

$$V=Ma=33.5M\sqrt{460+t}$$

The effective drag of the various component parts of the airplane is presented in figures 14 to 27. It will be noticed that the nacelle-drag data given in figures 15 to 21 were obtained only with natural transition on the smooth models. As previously stated, these data are not quantitatively applicable to flight conditions where extensive laminar layers do not exist, unless the correction factors developed in the appendix are applied. Figures 15 to 21 as they stand are intended to show critical speeds and to permit qualitative comparisons of the various arrangements.

The contribution of the various component parts to the total drag of the standard and the improved models is shown in figures 28 and 29. The percentage drag of the various parts is summarized in table II for the conditions of both natural and fixed transition. The drag of the complete standard model and the improved model is shown in figure 30.

The effect on lift of the various components is given in figure 31 for three representative speeds. The nacelles in the high and the low positions, respectively, increased and decreased the lift at a given attitude. The addition of fuselage and tail decreased the lift at angles below 2° and increased the slope of the lift curve.

The pitching-moment coefficients computed about the quarter-chord point of the mean aerodynamic chord (approximate center-of-gravity location of actual airplane) are given in figure 32 for the complete models. There were no marked compressibility effects. Correction for the tip sections of the wing omitted on the model would make the values of $dC_m/d\alpha$ more negative than indicated from the figure.

Figures 33 to 36 in the appendix show the effect of the location of the boundary-layer transition point on nacelle drag; figures 37 and 38 give factors for correcting the nacelle-drag data obtained with natural transition (figs. 15 to 21) to the fixed-transition condition.

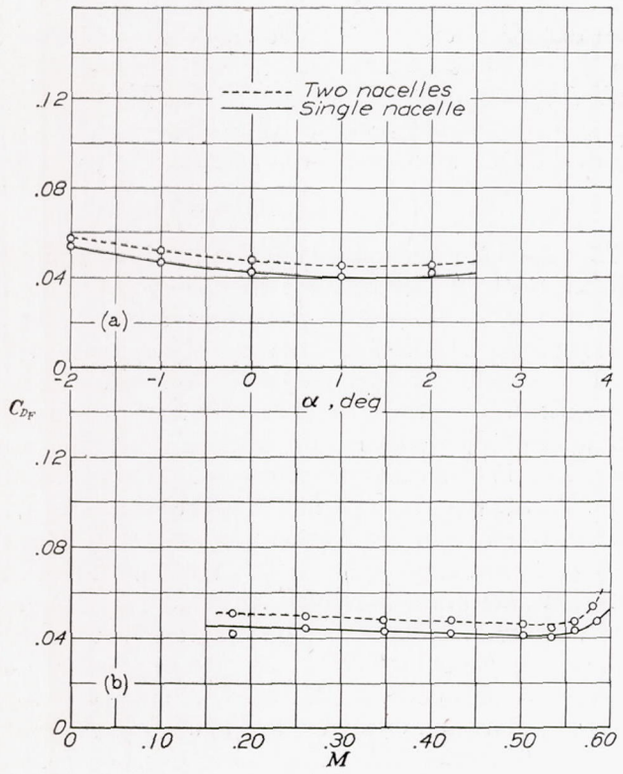

(a) R=3,310,000; M=0.35.
(b) α=0°.

FIGURE 14.—Interference between nacelles on wing without fuselage. Standard nacelles in normal position. Wing with transition fixed at 10-percent chord.

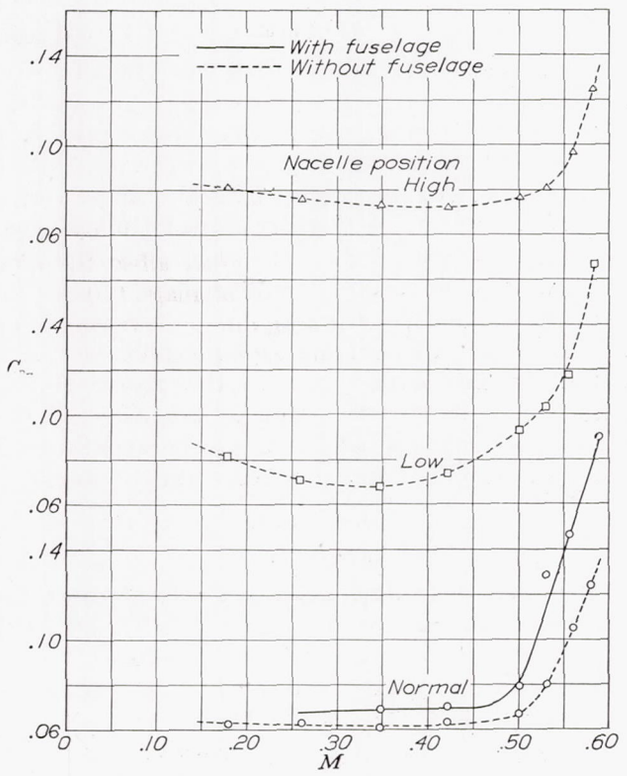

FIGURE 16.—Effect on critical speed of vertical location of nacelles and of presence of fuselage. Standard nacelles without cooling air. Wing with natural transition. α=−2° (α_n=−4°).

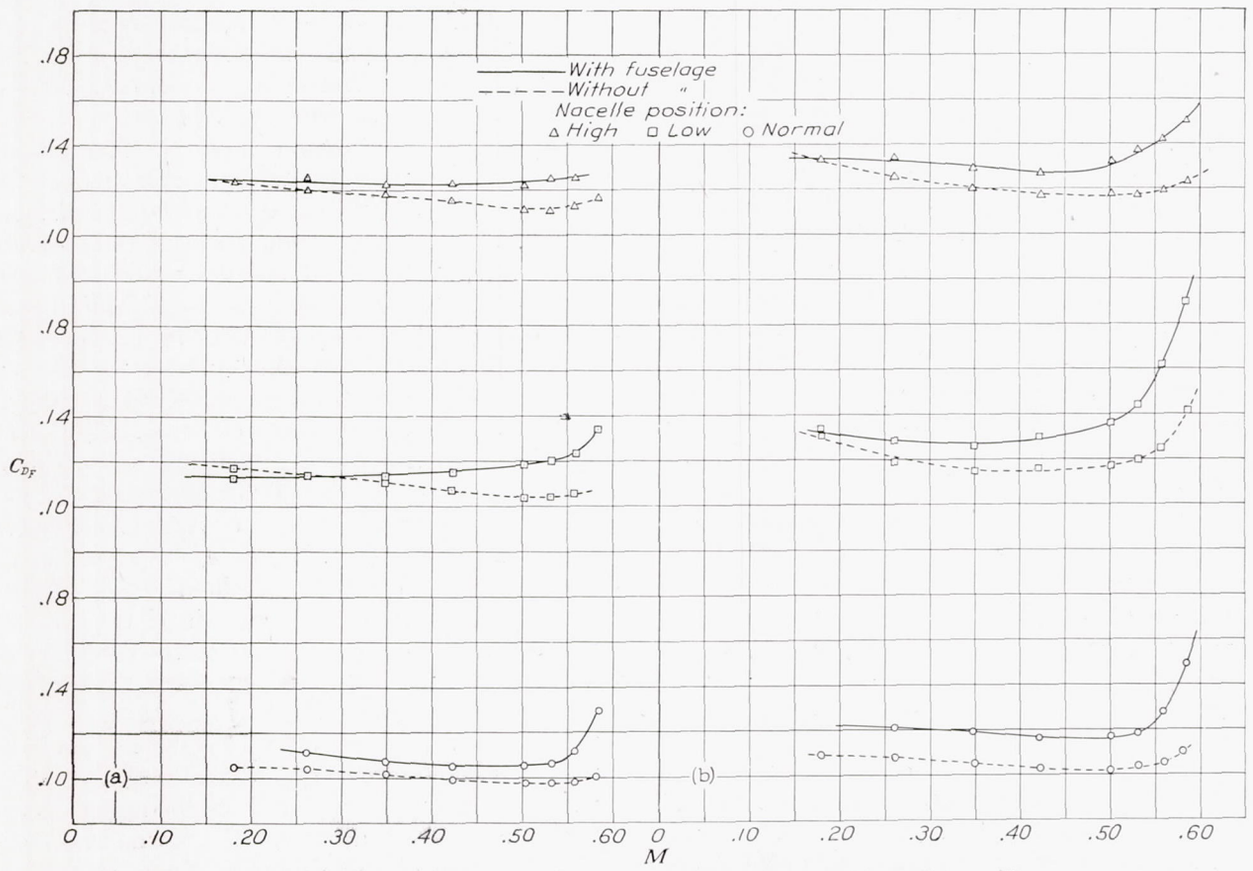

(a) α=0° (α_n=−2°).
(b) α=−2° (α_n=−4°).

FIGURE 15.—Effect on critical speed of vertical location of nacelles and of presence of fuselage. Standard nacelles with cooling air. Wing with natural transition.

PRECISION

The force-test results are uncorrected for tunnel-wall effects with the exception of the effective fuselage drag, to which a buoyancy correction of about 5 percent was applied. The effect of buoyancy on the wing and the nacelle drag was negligible. The interference at the juncture of wing and tunnel wall could not be determined but apparently did not seriously affect the wing drag, which is of the right order of magnitude. The inflow over the ends of the wing due to leakage at high lifts made the determination of maximum lift rather doubtful. The data shown in this report therefore extend only to $C_L=0.6$. The jet-boundary effect on critical speed is considered secondary because the frontal area of the model is only 6 percent of the jet area.

DISCUSSION

NACELLE DRAG

Interference between nacelles on wing without fuselage.—For the sake of accuracy, most of the nacelle-drag data were obtained with two nacelles, normally spaced four diameters apart, on the wing without the fuselage. There was a slight interference between the nacelles (fig. 14) amounting to $\Delta C_{D_F}=0.005$, which was approximately constant throughout the speed and the angle-of-attack ranges. The drag data obtained without the fuselage should be reduced by this amount if comparisons with tests employing a single nacelle are made. As previously stated, the results shown in figure 14 obtained with fixed transition on the model wing (transition on the standard nacelles occurred naturally at the point of sharpest curvature of the nose) are applicable to flight conditions after suitable Reynolds number corrections have been made. The nacelle drag shown in figures 15 to 21 was much higher than that shown in figure 14. This increase is due to the fact (see appendix) that these results (figs. 15 to 21) were obtained on smooth models with natural transition; they are presented only to show critical speeds and to permit qualitative comparisons.

Nacelle critical speeds.—The critical speed, at which the effective nacelle drag coefficient begins to increase abnormally, is affected by any factor that changes the ratio of maximum local velocity to stream velocity. The principal factors are angle of attack, interference effects, and cooling-air flow. Figures 15 and 16 show that the influence of these variables results in a range of critical speeds for the standard nacelles from about $M=0.47$ to beyond the range of the tests. The rate of increase of drag beyond the critical speed is generally so severe that the top speed of the airplane could not economically be much greater than the critical speed of the nacelles. As previously discussed, the critical flying speed corresponding to the critical value of M depends on the air temperature. Thus, at high altitudes where low temperatures are encountered, the flying speed at which the shock forms will be lower than at sea level. Since airplane top speeds tend to increase with altitude, the danger of encountering serious compressibility effects is very real. At 15,000 feet in standard atmosphere, for example, $t=5°$ F and $a=723$ miles per hour. The critical flying speed corresponding to the lowest critical Mach number for the nacelles, 0.47, would be

$$V_{cr}=M_{cr}\times a=340 \text{ miles per hour}$$

The results of reference 11 show that the effect of the slipstream of a conventional tractor propeller on the velocity distribution over a good cowling is slight for the high-speed condition. In some instances, the effect of the propeller slightly increased the maximum local velocities but in others the peak velocity was decreased. It appears conservative to assume that the peak velocity will be increased by the amount of the propeller slip. In the absence of pertinent propeller-test data, the slip in the present application was estimated from the power requirements at $M=0.50$. When uniform thrust distribution was assumed along the blade, the computed slip velocity immediately behind the propeller was $0.02V$. In order to allow for the fact that the actual thrust distribution is not uniform, this value was increased by 50 percent, giving an estimated maximum slip velocity of $0.03V$. The critical Mach numbers shown herein for the nacelles and the wheels may therefore be reduced by about $\Delta M=0.03$ owing to tractor-propeller interference.

If the effect of angle of attack on critical speeds is next considered, it can be seen from figure 15 that the critical speeds at $\alpha=-2°$ (nacelle angle of attack $\alpha_n=-4°$ to flight path) were markedly lower than at $\alpha=0°$ ($\alpha_n=-2°$). According to reference 5, this effect is due to an increase with angle of attack of the peak local velocities at the cowling nose. The minimum peak velocity occurs when the nacelle axis is parallel to the flight path. Extrapolation of the results of figure 15 shows that, by a proper alinement of the nacelles, the critical speed would be advanced beyond the range of the test speeds. This result emphasizes the fact (discussed in more detail in reference 5) that, for high-speed flight, the nacelle axes must be alined with the relative wind.

A secondary effect of the propeller slipstream would be to alleviate the indicated effects of angle of attack on nacelle critical speeds. This effect is undoubtedly small and can conservatively be neglected.

The effect on critical speed of vertical location of the standard nacelles (figs. 15 and 16) is probably due to the change in lift with nacelle location. With the nacelles in the low position, the lift of the combination was decreased, thereby increasing the downflow at the cowling nose, which was already operating at a negative angle. The effective angle of attack was thus augmented and the critical speed for the low position was made lower than for the normal position. The lift was increased with the nacelle in the high position and the accompanying upflow at the cowling nose slightly decreased the effective negative angle of the nacelle; the critical speed was thereby advanced beyond that of the normal position.

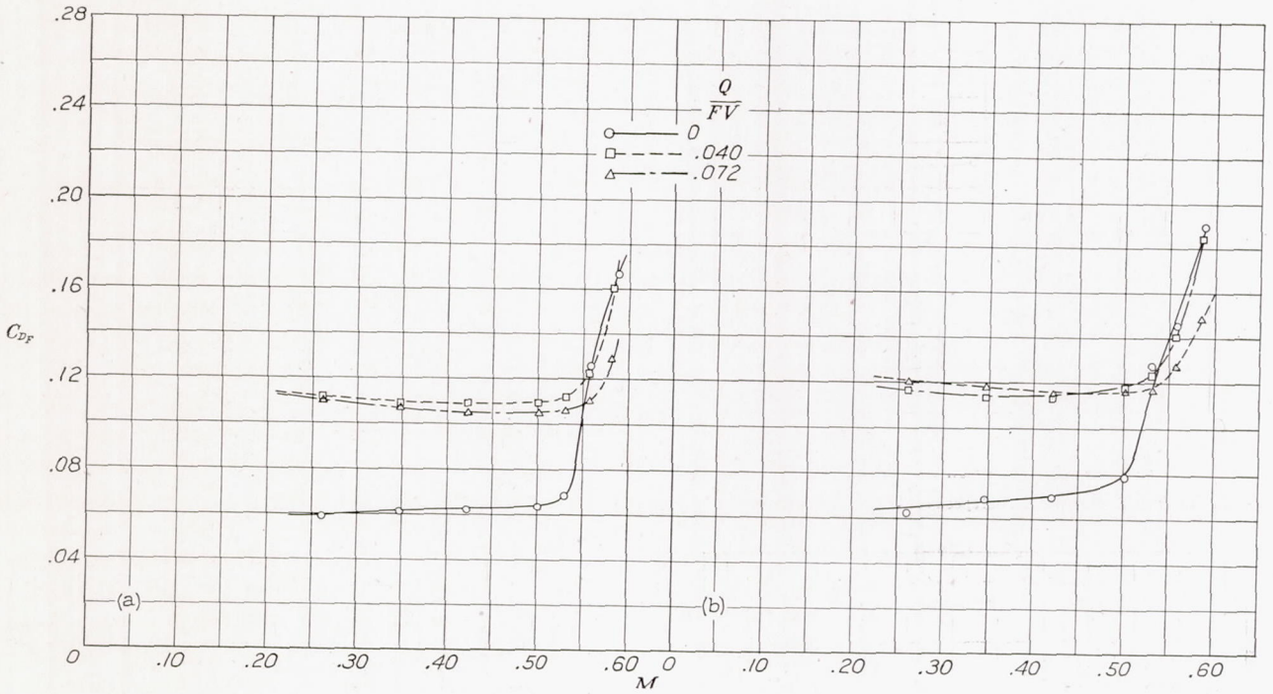

(a) $\alpha=0°$ ($\alpha_n=-2°$). (b) $\alpha=-2°$ ($\alpha_n=-4°$).

FIGURE 17.—Effect on critical speed of air flowing through cowling. Standard nacelles with fuselage. Wing with natural transition.

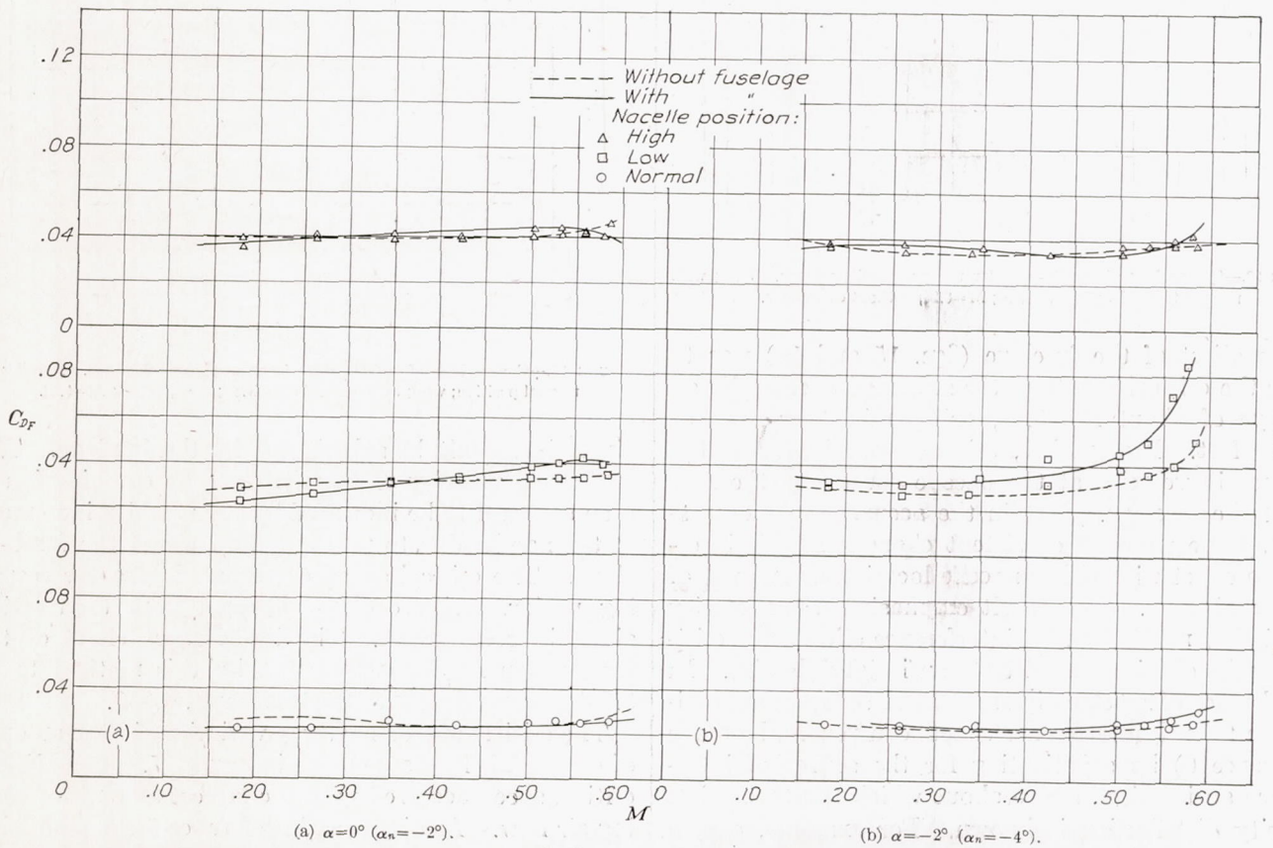

(a) $\alpha=0°$ ($\alpha_n=-2°$). (b) $\alpha=-2°$ ($\alpha_n=-4°$).

FIGURE 18.—Effect on critical speed of vertical position of nacelles and presence of fuselage. Streamline nacelles. Wing with natural transition.

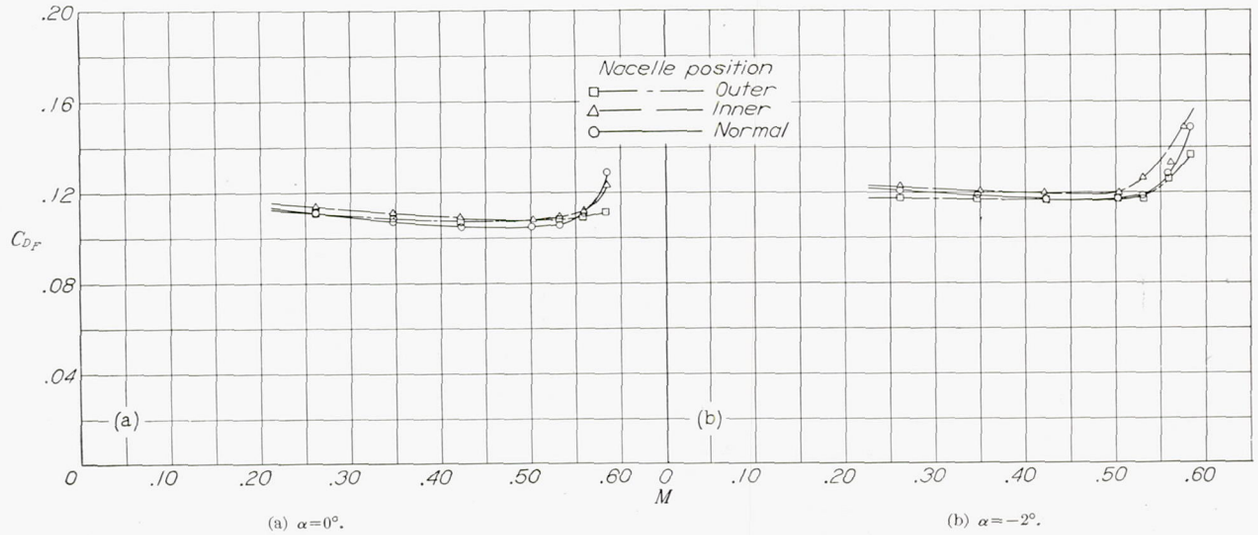

(a) $\alpha=0°$. (b) $\alpha=-2°$.

FIGURE 19.—Effect on nacelle drag and critical speed of lateral position of nacelles. Standard nacelles with cooling air. Wing with natural transition. (In presence of fuselage.)

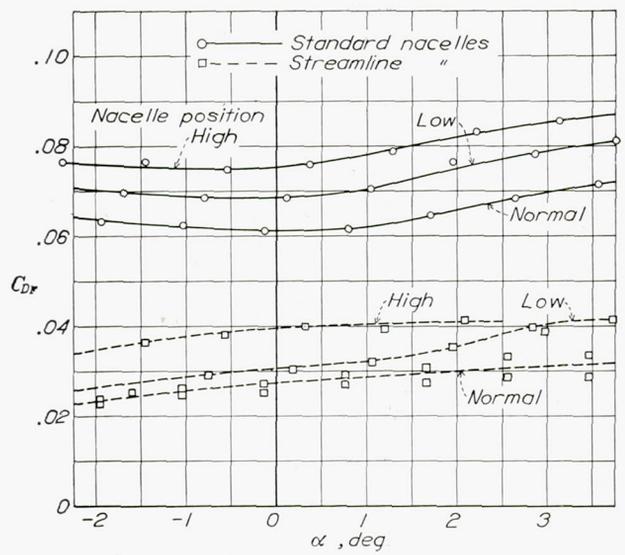

FIGURE 20.—Comparison of nacelle drag for three vertical positions. Wing with natural transition; $R=2{,}550{,}000$; $M=0.26$; without cooling air.

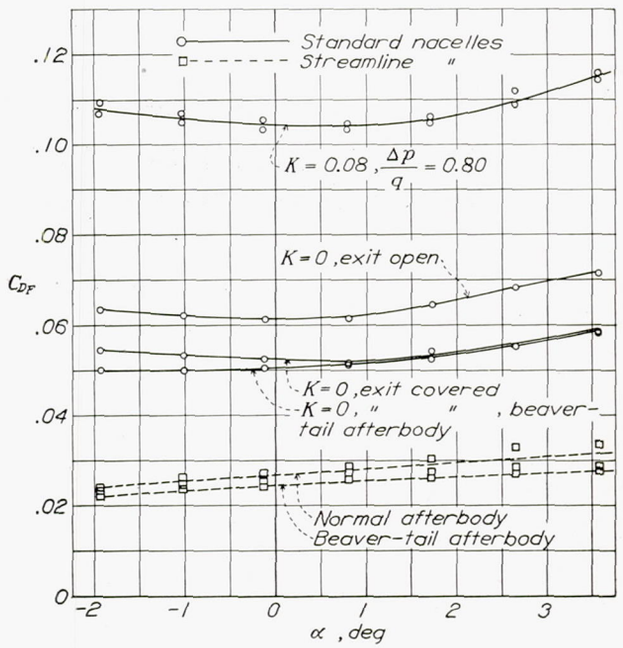

FIGURE 21.—Comparison of nacelle drag for several modifications. Nacelles in normal position; wing with natural transition; $R=2{,}550{,}000$; $M=0.26$.

The effect of the fuselage (figs. 15 and 16) was to lower the critical speeds of the standard nacelles by an average of about $M=0.03$, or 22 miles per hour at 15,000 feet. Presumably, this decrease is due to the increase in velocity at the nacelle caused by the flow about the fuselage. Within the accuracy of measurement, there were no consistent changes in this interference effect with either nacelle location or amount of cooling-air flow. This result emphasizes the necessity of suitably modifying, for interference effects, the critical speeds obtained from tests on isolated bodies. In the absence of specific high-speed test data, an approximation to such interference effects can usually be made (reference 6) by substituting for the source of interference an idealized shape about which the theoretical velocity distribution is known. For example, one of the bodies of revolution of reference 10 of comparable dimensions could be substituted for the fuselage. The peak local velocity of the wing-nacelle combination is then assumed to be increased by the velocity increment at the nacelle due to potential flow about the fuselage alone. The critical speed corresponding to the resulting peak velocity can be obtained from the relation given in reference 6. The interference effect of the fuselage on M_{cr} was computed by this method to be 0.025 as compared with the test result, 0.030.

The critical speeds for three variations in the amount of cooling-air flow are shown in figure 17. The highest critical speed occurred with the largest amount of cooling-air flow. As discussed in reference 5 the admission of air into the cowling tends to relieve the external

velocity peak at the cowling nose, thereby advancing the critical speed. It will be subsequently shown that these slight gains in critical speed are obtained at the expense of an excessive amount of cooling-air flow for high-speed conditions and that the resulting high nacelle drag is a more serious consideration than the advance in critical speed. More effective means of advancing the critical speed are proper alinement of the nacelle and reduction in the curvature of the cowling nose, as discussed in reference 5. The nacelle drag throughout the speed range is reduced by these modifications.

The critical speed of the streamline nacelles (fig. 18) was beyond the highest test speed, which corresponded to $M=0.58$. The theoretical velocity distribution about a similar body indicates a value of M_{cr} greater than 0.80 for the extreme attitude tested ($\alpha_n=-4°$). The abnormal increase in drag in the low position for $\alpha=-2°$ is probably due to the formation of a compression shock on the lower surface of the wing as a result of interference at the wing-nacelle juncture. The theoretical excess velocities on wing and nacelle for this attitude when added indicate a critical M of 0.56, which is in good agreement with the test results (fig. 18 (b)). The additional interference effects of the fuselage lowered the critical M to roughly 0.54. In the high and the normal positions, the effect of increase in lift over the lift in the low position sufficiently reduced the local velocities on the lower surface of the wing to delay the shock on the wing to beyond the range of test speeds.

The effects of lateral location (fig. 19) on critical speed were small. In general, the inner position had slightly lower critical speeds than the normal and the outer locations owing to the increased fuselage interference effect.

Nacelle drag at subcritical speeds.—The normal nacelle location had the lowest drag of the three vertical locations for both the standard and the streamline nacelles (fig. 20). The high position had the highest drag. Of the lateral locations (fig. 19), the drag with the normal position was less than that with the inner position and equal to or less than that with the outer position. The relative merit of the positions did not change with nacelle attitude or with speed.

Consideration should be given to the effect of the propeller on the efficiency of the various nacelle locations. As previously mentioned, the effect of the propeller slipstream at high speeds is small and of the same order of magnitude for all positions. More important is the variation of propulsive efficiency with position. No test data are available for small vertical displacements, but the results of reference 13 for large changes in nacelle location were interpolated to estimate the effects. The indicated propulsive efficiency for the normal position is 1 percent greater than for the high position but ½ percent lower than for the low position. Inasmuch as the low position of the nacelles would increase the drag of this airplane by 2 percent, the ½-percent gain in thrust at a given speed would be more than offset. There were no appreciable differences in maximum lift for the various nacelle locations. The relative merit of the nacelle positions is therefore unchanged by consideration of propeller effects and maximum lift; the normal position is preferable to all others investigated.

The drag due to cooling-air flow through the standard nacelles amounted to more than one-half the total nacelle drag (fig. 21). The increment due to cooling was approximately constant for all test conditions; the average value was 0.057, which agrees well with the data of references 11 and 14 for similar conductance and exit opening. As figure 21 shows, a part of this increment is due to the surface discontinuity at the exit opening because, with the air stopped but with the exit slot open as is usual, the drag-coefficient increment due to the exit slot alone was 0.011. As is shown in references 11 and 14, however, the drag variations with changes of the exit opening are properly included in the cooling drag because the usual and the most efficient method of controlling the cooling-air flow is to vary the width of the exit-slot opening.

The large saving in nacelle drag that may be effected by passing exactly the correct amount of cooling air through the cowling at every speed by means of a variable exit-slot opening has been fully discussed in references 11 and 14. On the airplane under consideration, the fixed exit slot provided sufficient cooling pressure drop at about 140 miles per hour but, as the speed was further increased, the amount of cooling air and the corresponding drag became increasingly excessive. At $M=0.30$, the design high speed, and with the exit slot properly reduced in size, the computed increment to nacelle drag for sufficient cooling is 0.009 (reference 14, $K=0.08$), resulting in a total necessary nacelle drag of only 0.045 instead of the measured value, 0.093. (Fixed transition, $\alpha=0°$, fig. 22.) The excessive cooling drag amounted to about 7 percent of the total airplane drag at $M=0.30$ and emphasizes the necessity of using cowling flaps or a similar means of controlling the flow of cooling air at high speeds.

A comparison of the nacelle drags with the normal and the beaver-tail afterbodies is also shown in figure 21. The differences were small.

In figure 22 is shown a comparison between the standard and the streamline nacelles applicable to flight conditions, that is, with transition fixed on nacelles and wing. Only the effects of nose shape are compared; there is no cooling-air flow and no exit slot for the standard nacelles. The drag of the streamline nacelles decreases from about 10 percent less than that of the standard nacelles at $R=1{,}000{,}000$ to about 30 percent less at $R=4{,}000{,}000$. Reference 5 shows that the drag of NACA cowled nacelles can be materially reduced by

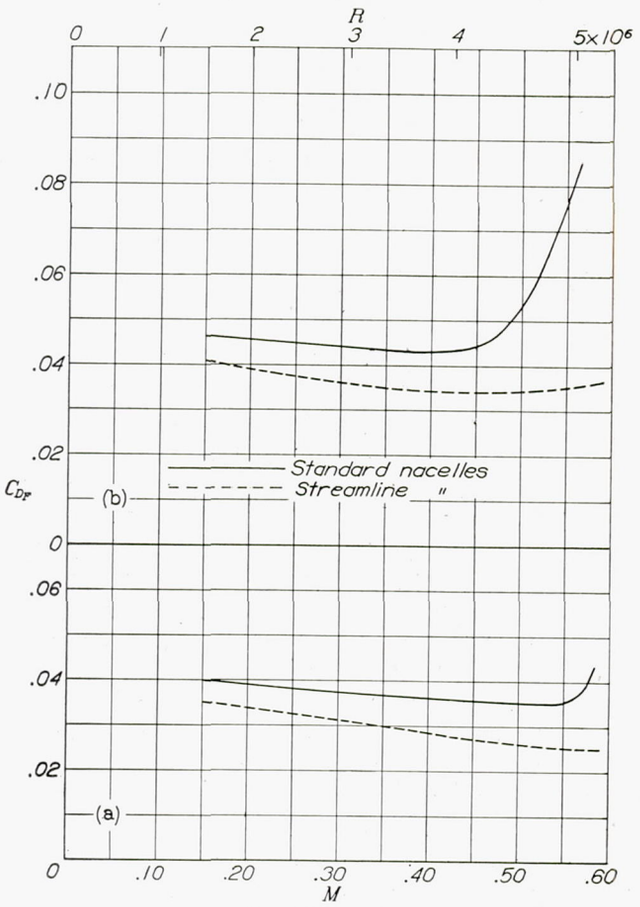

(a) $\alpha=0°$ ($\alpha_n=-2°$).
(b) $\alpha=-2°$ ($\alpha_n=-4°$).

FIGURE 22.—Comparison of nacelle drag with standard cowling (exit slot covered, $K=0$) and with streamline nose. Fixed transition on nacelles and wing.

decreasing the curvature of the cowling nose. It therefore appears that, if the standard cowling nose in the present tests were replaced by a better nose shape, such as C of reference 5, the streamline nacelles would have little advantage over the standard nacelles in the low Reynolds number range of these tests. Apparently, at low Reynolds numbers, the increase in wetted area of the streamline nacelles nearly offsets the reduction in form drag. At high Reynolds numbers, the reduction in form drag with the streamline nose would probably be greater than the differences in skin-friction drag, giving the streamline nacelles greater advantage over the best possible NACA cowling shape.

The presence of the fuselage exerted a consistently unfavorable interference effect on nacelle drag (figs. 15, 16, and 18).

An unexpected small increase in effective nacelle drag occurred as a result of interference between the nacelles and the tail group (fig. 23). The drag of the tail group, with and without nacelles, is also shown in the figure to verify the nacelle-drag results. This effect may be due to disturbance of the extensive laminar boundary layer of the tail by spreading turbulence from the nacelles and, if so, would not exist in flight. Observations of a very thin dust pattern remaining on the tail surfaces after lengthy high-speed runs indicated that the laminar flow extended in some instances as far back as 70 percent of the tail chord except in the immediate proximity of the fuselage.

In the conclusion of the discussion of nacelle drag, it should be pointed out that the optimum conditions for high critical speed, alinement with the relative

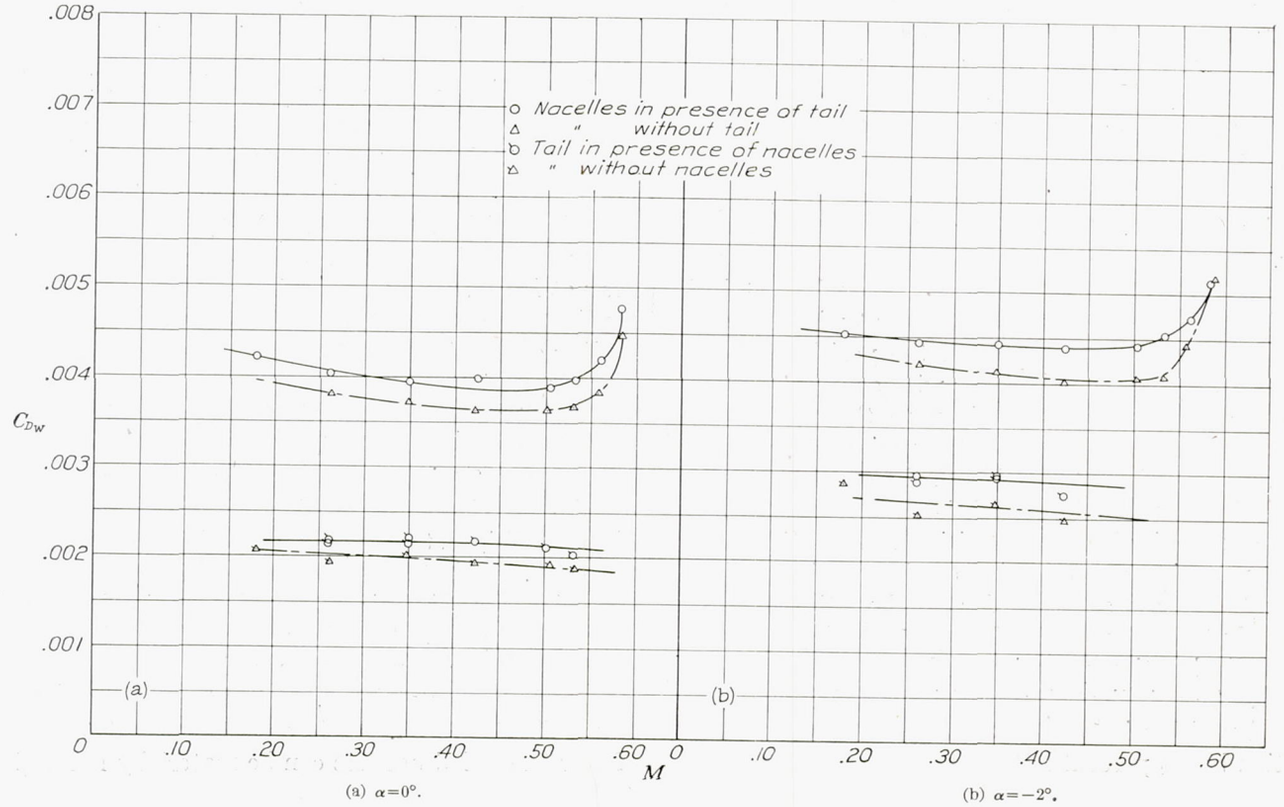

(a) $\alpha=0°$.
(b) $\alpha=-2°$.

FIGURE 23.—Nacelle and tail drag data showing unfavorable interference between nacelles and tail. Standard nacelles with cooling air; wing and tail with natural transition.

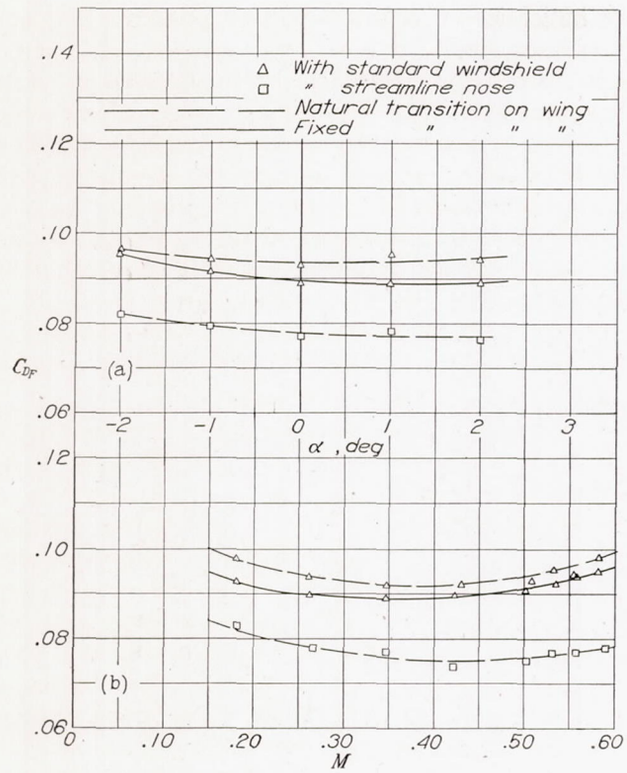

(a) R=3,310,000; M=0.35.
(b) α=0°.

FIGURE 24.—Drag of fuselage with fillet.

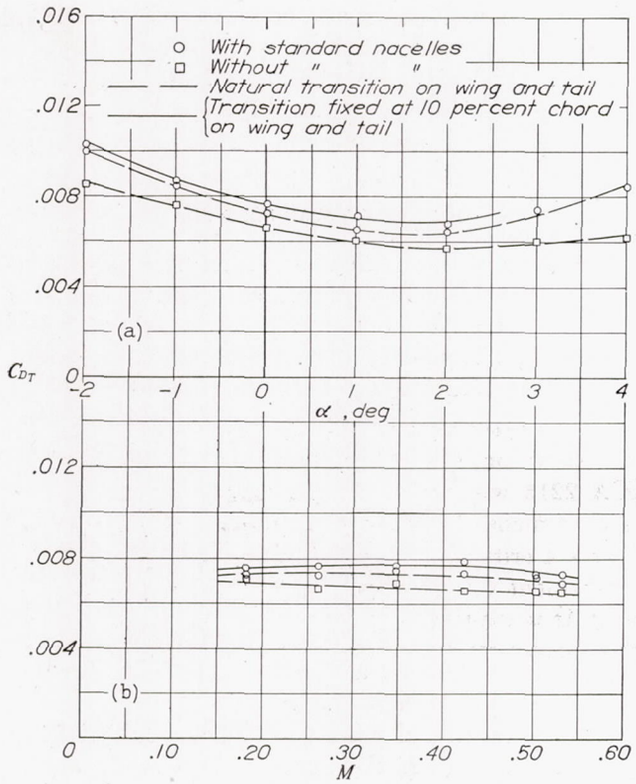

(a) R=2,550,000; M=0.26.
(b) α=0°.

FIGURE 26.—Drag of tail group.

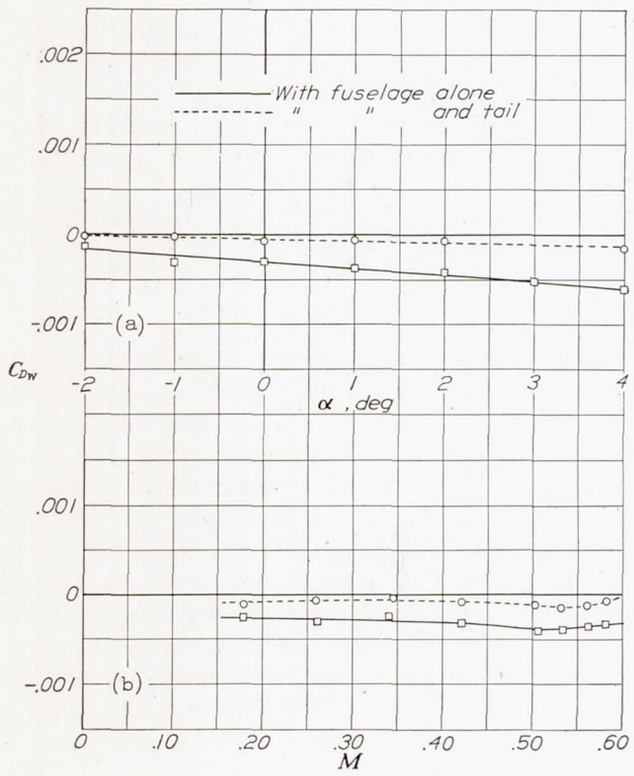

(a) R=2,550,000; M=0.26.
(b) α=0°.

FIGURE 25.—Drag of fillet.

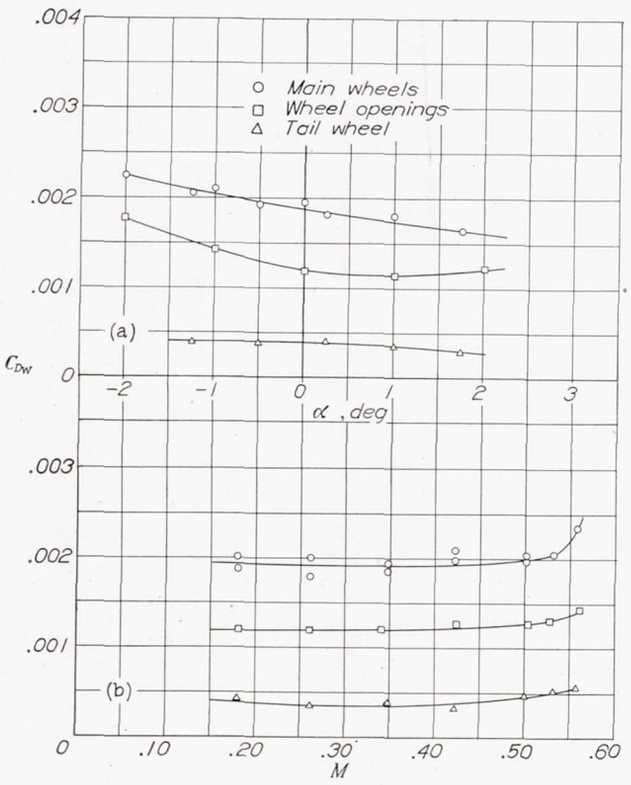

(a) R=3,310,000; M=0.35.
(b) α=0°.

FIGURE 27.—Drag of wheels and wheel openings.

wind and small curvature of the cowling nose, also permit the lowest nacelle drags at speeds below the critical. Likewise, interference effects that increase the local velocity at the nacelles not only lower the critical speed but also increase the drag at speeds below the critical.

DRAG OF FUSELAGE AND FILLET

The drag of the fuselage and fillet with the standard nose and windshield arrangement (figs. 1 and 4) and with the streamline nose completely faired over the windshield irregularity (figs. 1 and 12) is presented in figure 24 as a function of both Mach number and angle of attack. The critical speed was beyond the limit of the tests. A serious effect of the fuselage, however, is the lowering of the critical speed of the wing due to interference at the wing-fuselage juncture. An estimate based on the theoretical velocities about the NACA 2215 wing and about a body of revolution of general dimensions similar to those of the fuselage indicates a critical M of 0.60. If the additional velocity increment due to a nacelle is also considered, the critical M is reduced to 0.58.

The conventional windshield fairing added 21 percent to the drag of the fuselage with streamline nose (fig. 24, $\alpha=0°$, $M=0.35$). The effect of detailed intermediate modifications is given in reference 1, where it was found that the windshield drag can be reduced to 2 percent without completely fairing over the cockpit enclosure; that recessed windows add 7 percent more drag than flush windows; and that sharp edges add from 2 to 14 percent more drag than rounded edges.

The effective drag of the fillet was negative at all attitudes tested (fig. 25). There was a consistent unfavorable interference between the fillet and the tail group, probably due to increased velocities in the region of the tail resulting from the improvement in flow near the fuselage. No compressibility effects appeared to be associated with the fillet.

DRAG OF TAIL GROUP

The effective drag of the tail group (fig. 26) is composed of the minimum profile drag of the vertical surfaces plus the profile and the induced drag of the horizontal surfaces and the interference effects. Because of the small Reynolds number and the thin sections of the tail, extensive laminar boundary layers are to be expected. The low minimum drag coefficient with natural transition is probably mainly due to these low-drag laminar layers. The fact that the addition of a 0.003-inch thread at 10 percent of the tail chord increased the minimum tail drag only 9 percent indicates that these threads were not sufficiently thick to cause a complete transition. This result is in agreement with the indication of the dust-pattern observations previously mentioned.

An increase of Mach number made no appreciable change in the effective tail drag. The airfoil sections employed were somewhat similar to the NACA 0009–64 which, at low angles of attack, has a critical speed greater than $M=0.80$ (reference 3). No marked interference effects on critical speed should occur, owing to the low local-velocity increments on the fuselage at the tail location.

DRAG OF WHEELS AND WHEEL OPENINGS

The high drag (fig. 27) of the main wheels in the retracted position (fig. 11) was largely due to disturbance of the flow about the afterbody of the nacelle. The effective drag rapidly decreased as the angle of attack was increased because the pressure gradient became more favorable on the lower surface of the nacelle and thereby counteracted the tendency of the wheels to cause separation. The wheel openings alone had the same general effect as the wheels. In the actual airplane, the effect of the openings would probably be more serious as the inside of the opening is not closed off from the interior of the nacelle.

The value of M_{cr} for the main wheels in the retracted position was about 0.54. From a consideration of the theoretical flow over a sphere, the M_{cr} of an isolated wheel would be expected to be about 0.57 and, in conjunction with the nacelle, to be about 0.53. This result is another illustration of the possibility of satisfactorily estimating the interference effects on critical speed by the method of reference 6.

The drag of the unretracted tail wheel was about one-fourth the drag of the retracted main wheels. The critical speed for the tail wheel would be expected to be about $M=0.57$, which was beyond the range of the wheel-drag tests.

DRAG OF COMPLETE MODEL

A comparison of the effective drags of the various parts of the standard model is given in figure 28 and table II. There were no appreciable changes with speed in the drag of any of the component parts except for the wheels and the nacelles, on which compressibility shocks occurred. As previously discussed, the drag of the nacelles with a properly regulated flow of cooling air would be considerably reduced from the values shown in figure 28, and the critical speed would be slightly lowered. The large drag cost of the semi-retracted landing gear, 10 to 14 percent of the total drag, is emphasized in the comparison shown in figure 28. The gear should be fully retracted and the openings closed.

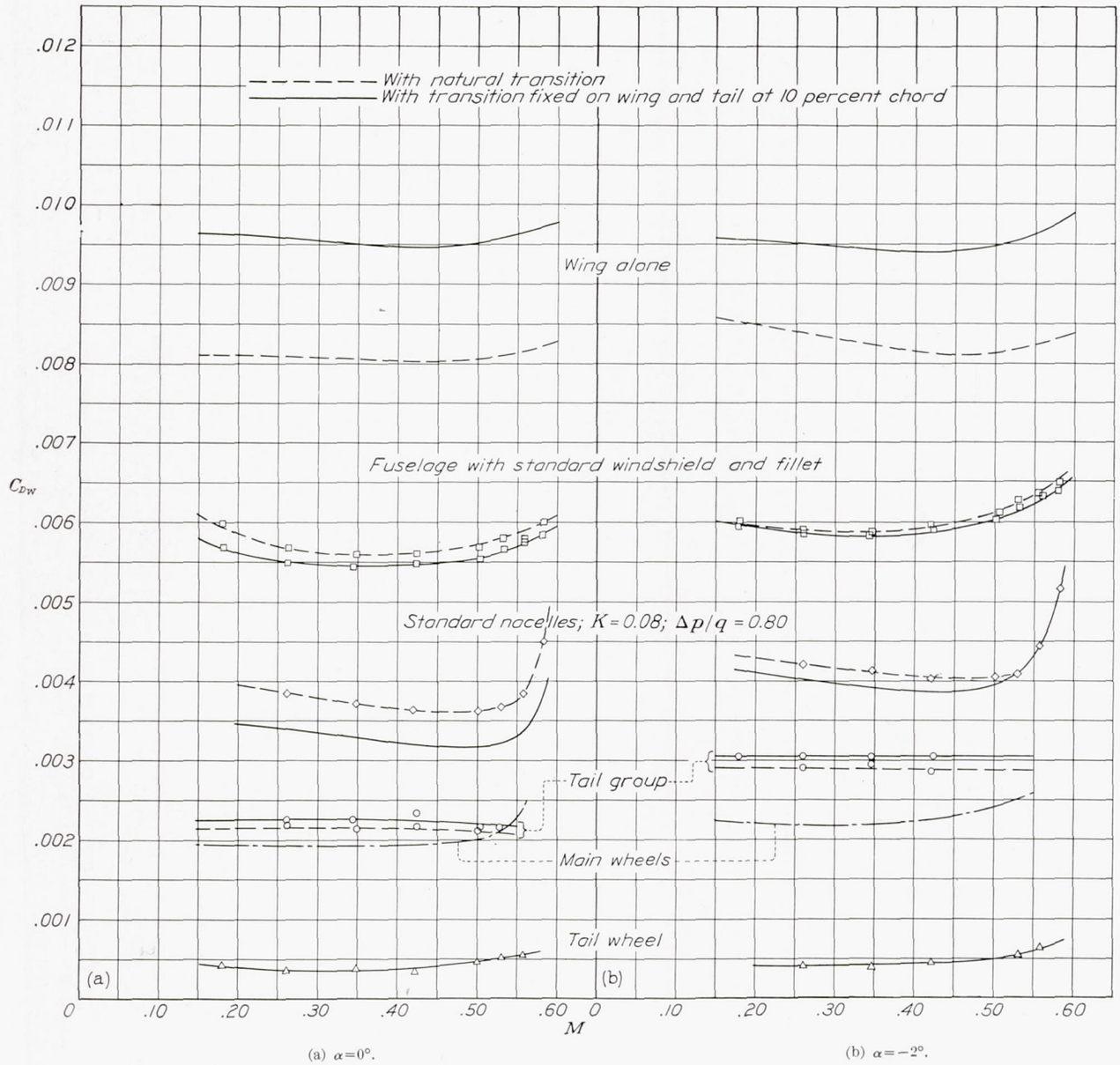

FIGURE 28.—Comparison of drag coefficients of principal parts of the standard model.

Figure 29 shows that no shock occurred on any part of the improved model in the range of the tests. The theoretical pressure distribution over the root section of the wing, modified for the interference effects previously discussed, indicates, however, that compression shocks will occur at the wing-fuselage and the wing-nacelle junctures at Mach numbers lower than 0.60. The critical Mach number of the wing alone is theoretically $M_{cr}=0.63$. It is therefore evident that the airplane, even with the indicated improvements, could not much exceed a value of M of 0.60 without suffering severe drag increases. A further advance in critical speed would involve the use of a thinner wing, of a wing of modified section, or, preferably, of both.

The drag-coefficient increment corresponding to an assumed adequate flow of cooling air for maximum power operation (pressure drop of 30 lb per sq ft across the engine) is also shown in figure 29. This drag was computed by the method of reference 14 for flight speeds up to the highest obtainable with the 850-horsepower-engine installation ($M=0.30$). At higher flight speeds, the maximum power output would have to be increased and, as shown in figure 29, the cooling drag coefficient would be constant with speed at about 2 percent of the airplane drag.

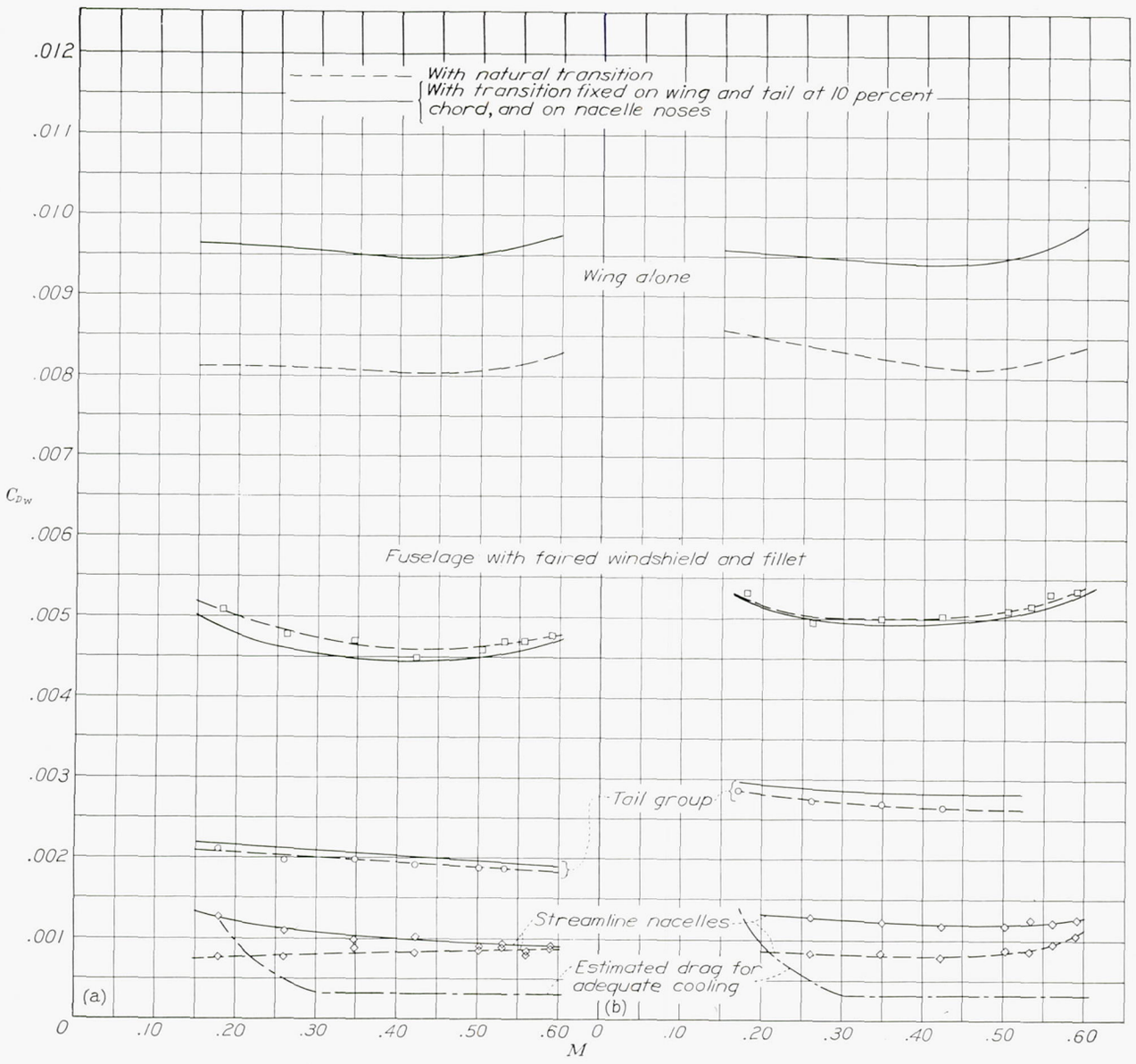

FIGURE 29.—Comparison of drag coefficients of principal parts of the improved model with faired windshield and streamline nacelles.

Figure 30 shows the total airplane drag for the standard and the improved models obtained by adding the effective drag of all the parts, as shown in figures 28 and 29. The difference in drag between the standard and the improved models includes only the drag due to excessive cooling-air flow in the standard nacelles plus the difference in drag between the standard and the streamline nacelles with zero cooling air, the drag of the landing gear, and the drag of the windshield. At a Mach number of 0.40, the improved model with fixed transition had 25 percent less drag. The increases in drag between $\alpha=0°$ and $\alpha=-2°$ occurred as a result of the increase in profile drag of all components due to increase in misalinement with the relative wind.

At a Mach number of about 0.40, the effect of compressibility on both models became sufficiently large to overbalance the reduction in drag with speed due to scale effect, the drag coefficients starting to increase slowly at this value of M. The results shown in figure 30 for the fixed-transition condition can be corrected for scale effect in the usual manner without accounting for changes in transition location.

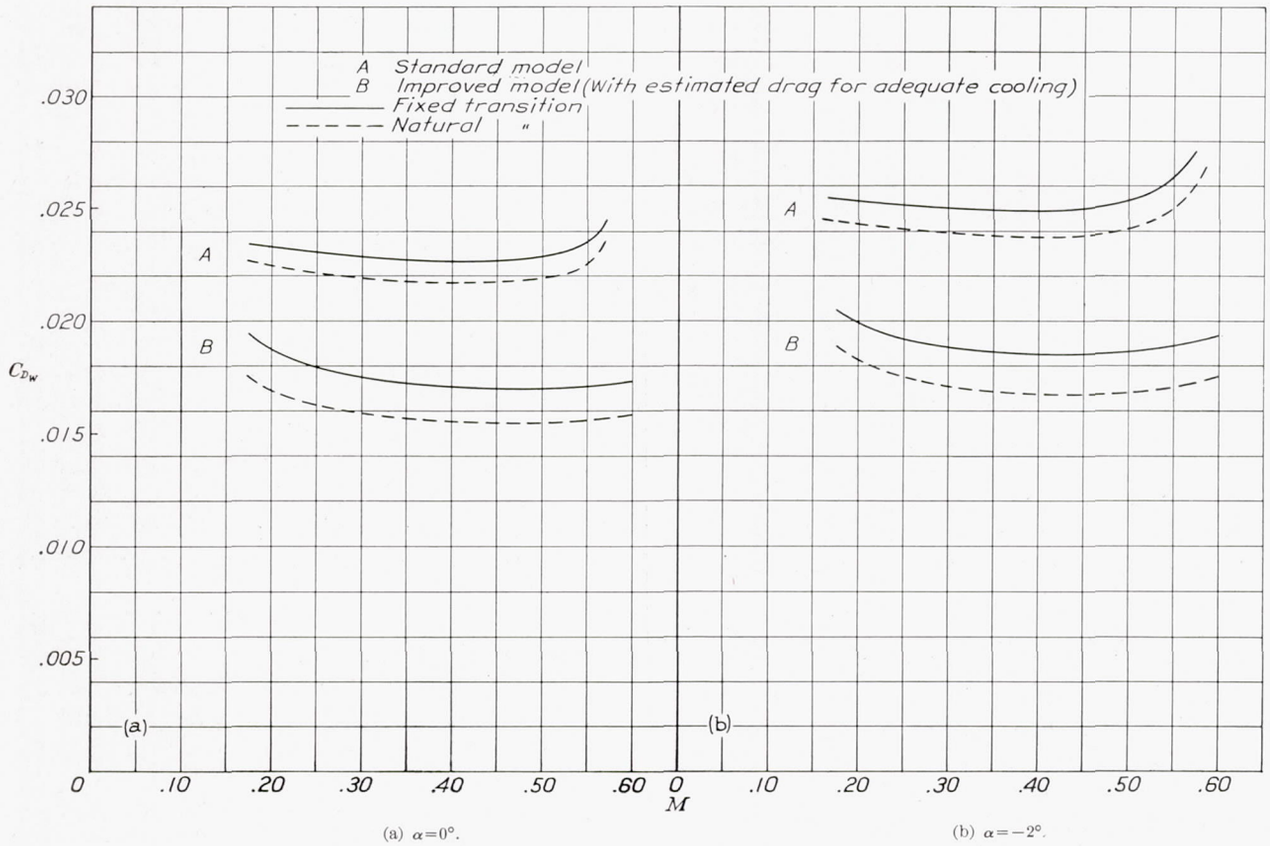

(a) $\alpha=0°$. (b) $\alpha=-2°$.

FIGURE 30.—Comparison of total drag of standard and improved models.

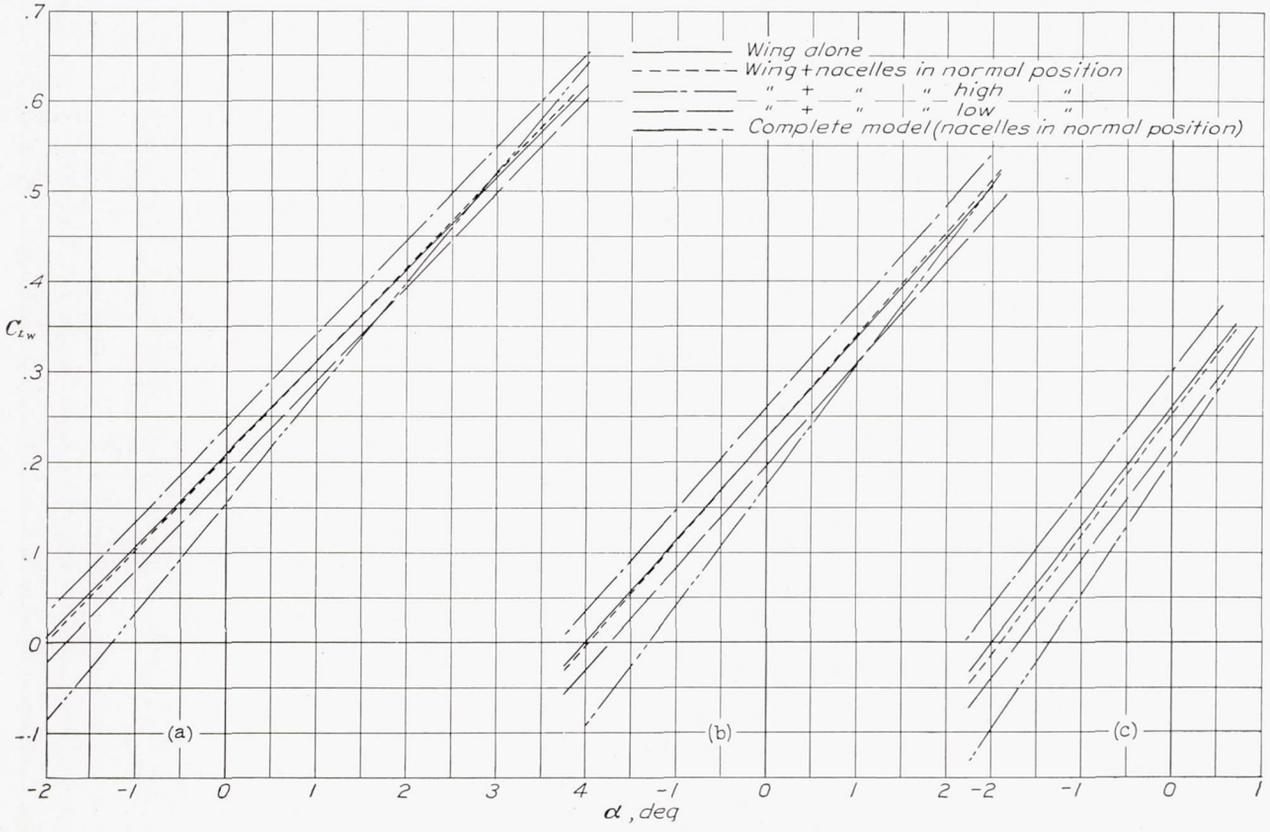

(a) $M=0.18$. (b) $M=0.35$. (c) $M=0.53$.

FIGURE 31.—Lift curves for wing and several combinations

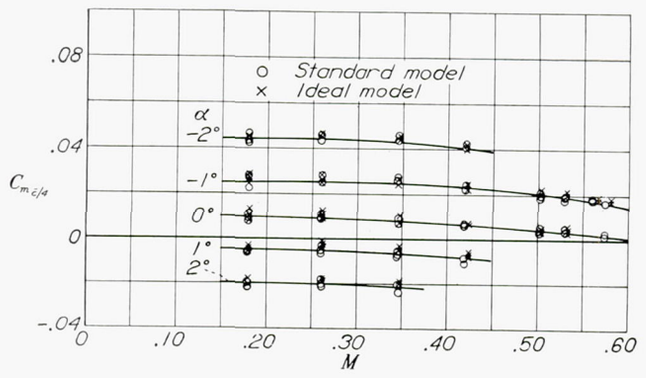

FIGURE 32.—Pitching-moment coefficients.

CONCLUSIONS

The following conclusions appear to be justified on the basis of the data obtained from tests made of the ⅛-scale model of a twin-engine low-wing transport airplane in the 8-foot high-speed tunnel:

1. The drag of a typical present-day transport airplane may be seriously increased at high speeds owing to the formation of compression shocks on the radial-engine cowlings at Mach numbers as low as 0.47 and on parts of the wing and partly protruding landing wheels at a Mach number of 0.54. The corresponding flight speeds at 15,000 feet (5° F) are 340 and 390 miles per hour. The estimated interference effect of the slipstream of a conventional tractor propeller might reduce these values by a Mach number of 0.03 or about 22 miles per hour.

2. The critical speeds obtained on the complete model were appreciably lower than the critical speeds of the isolated parts, owing to mutual interference effects among the various parts.

3. Components such as the nacelles and the fuselage should be alined with the relative wind in the high-speed condition so that the local velocities will exceed the general stream velocity by a minimum amount. Realining the nacelles on the model tested would advance the critical Mach number beyond 0.58.

4. The critical speed of the airplane can be advanced from a Mach number of 0.47 to a Mach number of about 0.60 by the alterations suggested. A further advance would, however, require fundamental changes, particularly the employment of a thinner wing or a wing of modified section.

5. The drag of the nacelles in the normal midwing location was less than that in the high position (with nacelle tangent to the lower wing surface), less than that in the low position (with nacelle tangent to the upper surface), and equal to or less than that in both the inner and the outer positions tested. Not only was the drag lowest for the normal position, but the critical speed was higher than for the low and the inner positions and virtually equal to the critical speeds in the high and the outer positions.

6. The advantage of streamline nacelles over standard NACA cowled nacelles is small at low Reynolds numbers but increases with Reynolds number because a larger favorable scale effect occurs on the streamline nacelles than on the standard nacelles.

7. Because of the lack of provision for regulation of the cooling air with speed, the drag of the standard nacelles was much greater than necessary.

8. The semiretracted landing gear contributed 12 percent to the drag of the complete model at subcritical speeds.

9. The fuselage with standard windshield accounted for 25 percent of the total drag. Fairing the windshield resulted in a decrease of 21 percent in fuselage drag, or about 5 percent of the total drag at a Mach number of 0.35.

10. The drag of the standard model was reduced 25 percent at a Mach number of 0.40 by removing the wheels and the openings of the semiretracted landing gear and by employing the streamline nacelles (with the estimated drag due to adequate cooling-air flow) and the fuselage with streamline nose.

LANGLEY MEMORIAL AERONAUTICAL LABORATORY,
NATIONAL ADVISORY COMMITTEE FOR AERONAUTICS,
LANGLEY FIELD, VA., *February 14, 1940.*

APPENDIX

THE EFFECT ON NACELLE DRAG OF THE LOCATION OF BOUNDARY-LAYER TRANSITION

In wind tunnels of low turbulence, the drag results obtained on smooth models will be misinterpreted unless detailed consideration is given to the condition of the boundary layer. The existence of extensive laminar boundary layers on smooth models makes the relative drag of the various parts greatly different from the relative drag in flight and also makes impossible the employment of the usual methods of scale-effect correction based on the assumption that no appreciable laminar layers exist. The problem of obtaining wind-tunnel results applicable to flight conditions is somewhat simplified by the fact that the surfaces of present-day aircraft are generally not smooth or fair enough to sustain extensive laminar flow (references 8 and 9). The very large Reynolds numbers attained in flight might prevent extensive laminar layers on conventional airfoils even if the surfaces were ideally smooth. The disturbances created by the propeller would also tend to cause early transition on bodies located in the slipstream. It seems safe to assume, therefore, that the flight boundary layers on conventional wings and bodies are almost wholly turbulent except for very limited laminar-flow regions at the leading edges of the various parts. Methods will now be discussed of correcting to this assumed flight condition the drag data obtained with the smooth models in the present tests.

Figure 33 shows the effect on the wing boundary layer of adding a conventional nacelle, both for the full-scale and the wind-tunnel conditions. The flow over the area covered by the afterbody A_1 of the nacelle is turbulent in flight but laminar in the wind tunnel, with the result that the reduction in wing skin friction due to covering a part of the wing with the nacelle is less in the tunnel by the amount

$$qA_1\ (C_{f_{turbulent}}-C_{f_{laminar}})$$

In the 8-foot high-speed tunnel, the interference between wing and nacelle has been found to cause transition to take place on the wing starting at the leading edge and spreading at an included angle of about 15° toward the trailing edge (fig. 33). This phenomenon causes an unfavorable interference drag of magnitude

$$qA_2\ (C_{f_{turbulent}}-C_{f_{laminar}})$$

which does not exist in flight because there the flow over A_2 is already turbulent. The total increment of the effective nacelle drag in the wind tunnel as compared with flight is therefore:

$$\Delta D=q(A_1+A_2)\ (C_{f_{turbulent}}-C_{f_{laminar}})$$

If the points of transition are known for the tunnel as well as for the flight conditions, the correction to the tunnel results can be estimated from the preceding equation with sufficient accuracy for practical purposes.

In the present tests, the correction was experimentally obtained by comparing the results of tests of the smooth models with tests of the same models with transition fixed at the assumed flight locations. In the second tests, transition was fixed by means of a 0.009-inch thread doped on the wing at the 10-percent-

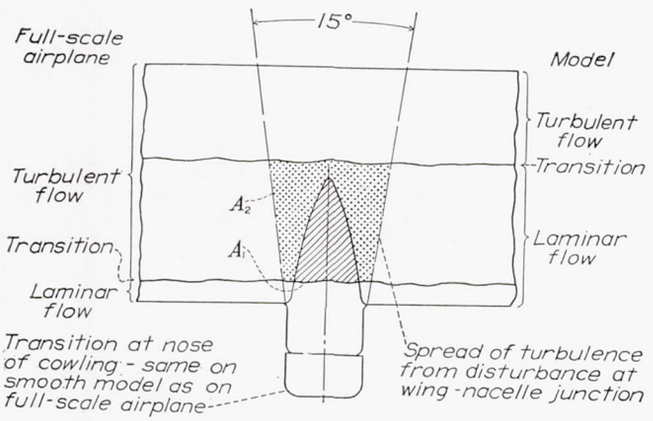

FIGURE 33.—Diagram showing differences in boundary-layer flow on model and full-scale wings, and area over which flow becomes turbulent on model owing to addition of nacelle.

chord location, on the standard nacelles at the point of maximum curvature of the cowling nose, and on the streamline nacelles at the probable location of the plane of intersection of a spinner and the nacelle proper. Figure 34 shows the drag of the standard nacelles with fixed transition on the wing to be from 10 to 35 percent less than that with natural transition, the amount depending on the angle of attack. The increase in this effect with angle of attack is due to a corresponding increase in the extent of the laminar layer on the lower surface of the wing. Figure 35 shows similar results obtained with the streamline nacelles.

Transition was found to occur for the standard nacelles at the point of maximum curvature of the cowling nose on the smooth model. Consequently, the addition of the thread to the cowling nose had no effect on the drag; but, with the streamline nacelles, the addition of the string to the nacelles nearly doubled the drag (fig. 35), indicating extensive laminar layers on the streamline nacelles. With transition fixed on the streamline nacelles, the decrease in drag due to fixing transition on the wing is shown to be almost equivalent to that of the standard nacelles throughout both the angle-of-attack and the speed ranges (fig. 36). This result is to be expected because, as previously shown (fig. 33), the effect is entirely due to the interference between the wing and the afterbody, which was the same for both nacelle-nose arrangements.

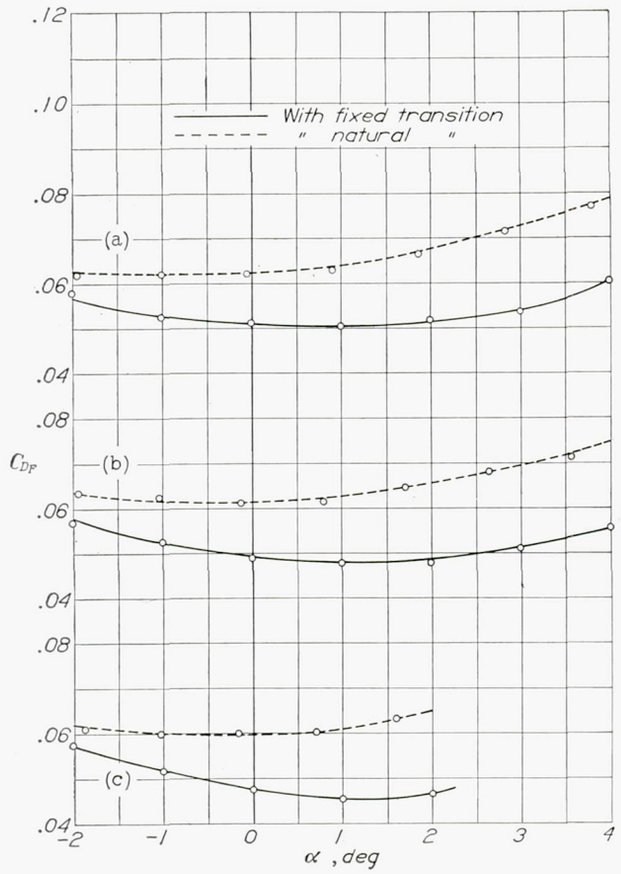

(a) R=1,780,000; M=0.18.
(b) R=2,550,000; M=0.26.
(c) R=3,310,000; M=0.35.

FIGURE 34.—Comparison of nacelle drag of standard nacelles (without cooling air) with natural transition on the wing and with transition fixed at 10-percent chord.

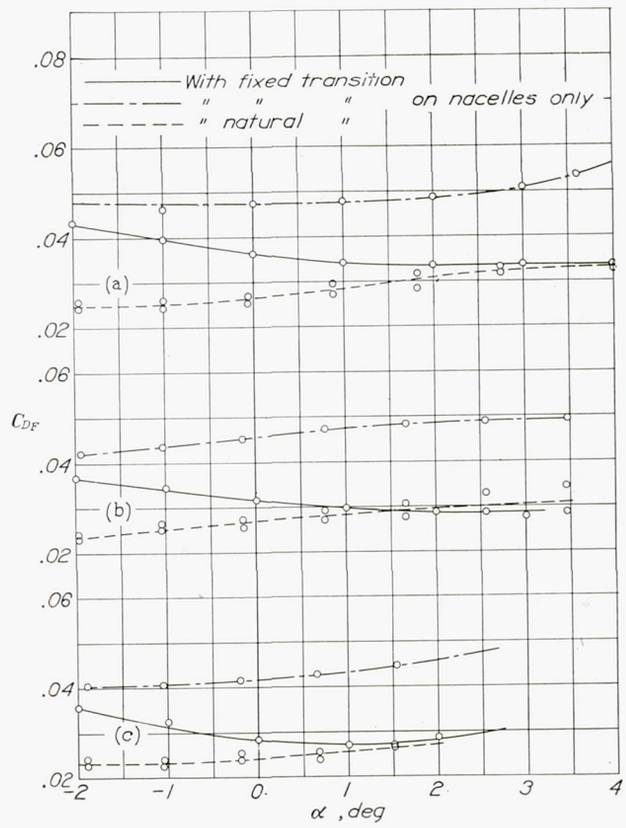

(a) R=1,780,000; M=0.18.
(b) R=2,550,000; M=0.26.
(c) R=3,310,000; M=0.35.

FIGURE 35.—Comparison of nacelle drag of streamline nacelles with natural transition on the wing and the nacelle, with fixed transition, and with fixed transition on the nacelles only.

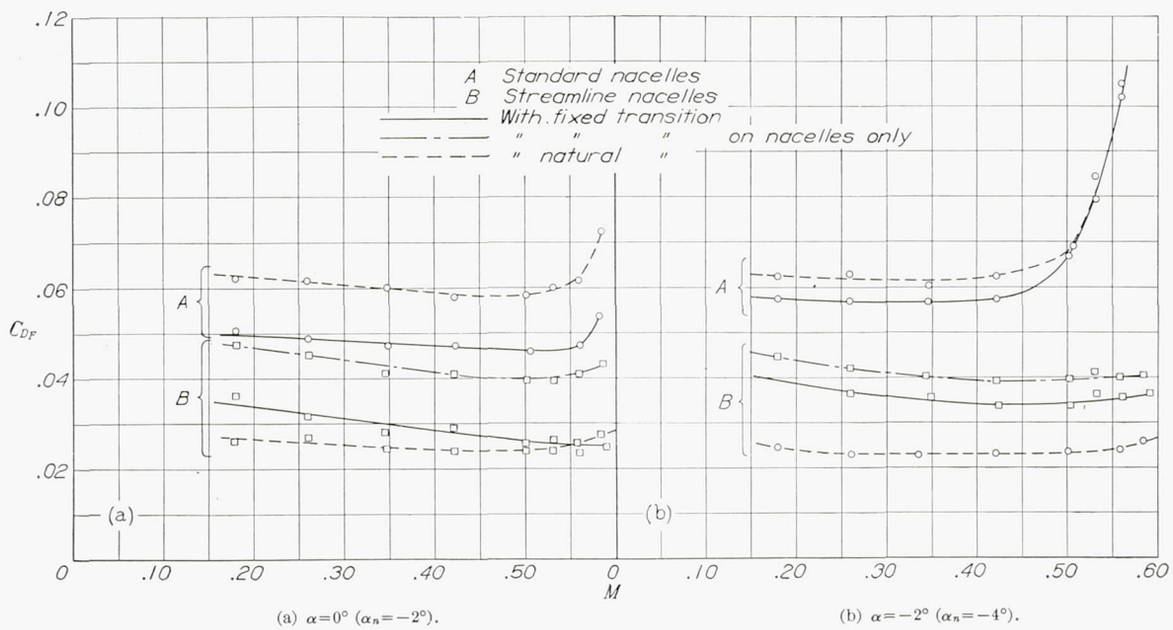

(a) α=0° (α_n=−2°).
(b) α=−2° (α_n=−4°).

FIGURE 36.—Comparison of nacelle drag with standard nacelles and with streamline nacelles with natural and fixed transition. Nacelles in normal position without cooling air.

The data of figures 34, 35, and 36 are condensed in figures 37 and 38 as correction factors to be added to the nacelle-drag data obtained with natural transition

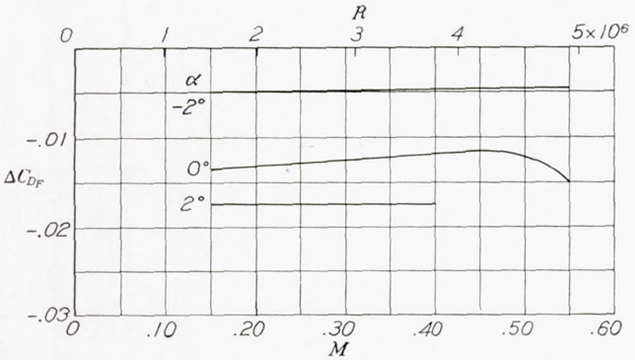

FIGURE 37.—Increment of drag coefficient of standard nacelles resulting from a change in the location of transition from the natural location on the smooth wing in the NACA 8-foot high-speed tunnel to 10 percent of the chord. No change in location of transition on nacelle.

$$\Delta C_{D_F} = C_{D_F}\begin{Bmatrix}\text{fixed}\\ \text{transition}\end{Bmatrix} - \Delta C_{D_F}\begin{Bmatrix}\text{natural}\\ \text{transition}\end{Bmatrix}$$

on wing and nacelles (figs. 15 to 21 and 23). The increment to be added to the drag of the standard nacelles (fig. 37) is due only to the changes in wing transition; it is negative in sign. The increment for the stream-

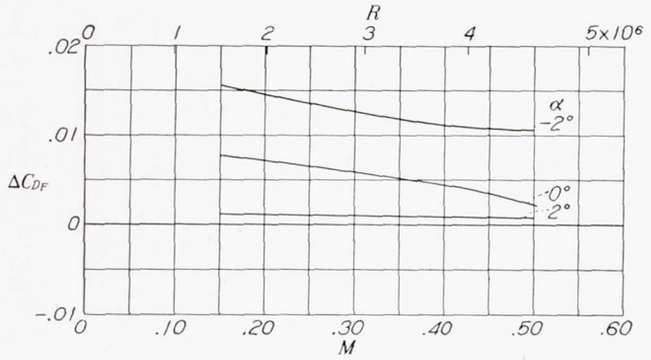

FIGURE 38.—Increment of drag coefficient of streamline nacelles resulting from a change in the location of transition on both wing and nacelles from the natural location in the NACA 8-foot high-speed tunnel to the fixed positions.

$$\Delta C_{D_F} = C_{D_F}\begin{Bmatrix}\text{fixed}\\ \text{transition}\end{Bmatrix} - \Delta C_{D_F}\begin{Bmatrix}\text{natural}\\ \text{transition}\end{Bmatrix}$$

line nacelles is positive (fig. 38) because the increase in skin friction on the nacelle more than offsets the effects of changes in wing transition. The correction factors were determined for the normal nacelle position, but they can probably be applied to the other positions with small error.

REFERENCES

1. Robinson, Russell G., and Delano, James B.: An Investigation of the Drag of Windshields in the 8-Foot High-Speed Wind Tunnel. Rep. No. 730, NACA, 1942.
2. Stack, John, Lindsey, W. F., and Littell, Robert E.: The Compressibility Burble and the Effect of Compressibility on Pressures and Forces Acting on an Airfoil. Rep. No. 646, NACA, 1938.
3. Stack, John, and von Doenhoff, Albert E.: Tests of 16 Related Airfoils at High Speeds. Rep. No. 492, NACA, 1934.
4. Lindsey, W. F.: Drag of Cylinders of Simple Shapes. Rep. No. 619, NACA, 1938.
5. Robinson, Russell G., and Becker, John V.: High-Speed Tests of Radial-Engine Cowlings. Rep. No. 745, NACA, 1942.
6. Robinson, Russell G., and Wright, Ray H.: Estimation of Critical Speeds of Airfoils and Streamline Bodies. Rep. (to be published), NACA.
7. Robinson, Russell G.: Sphere Tests in the N. A. C. A. 8-Foot High-Speed Tunnel. Jour. Aero. Sci., vol. 4, no. 5, March 1937, pp. 199–201.
8. Jones, B. Melvill: Flight Experiments on the Boundary Layer. Jour. Aero. Sci., vol. 5, no. 3, Jan. 1938, pp. 81–101.
9. Hood, Manley J.: The Effects of Surface Waviness and of Rib Stitching on Wing Drag. T. N. No. 724, NACA, 1939.
10. Abbott, Ira H.: Fuselage-Drag Tests in the Variable-Density Wind Tunnel: Streamline Bodies of Revolution, Fineness Ratio of 5. T. N. No. 614, NACA, 1937.
11. Theodorsen, Theodore, Brevoort, M. J., and Stickle, George W.: Full-Scale Tests of N. A. C. A. Cowlings. Rep. No. 592, NACA, 1937.
12. Hood, Manley J.: The Effects of Some Common Surface Irregularities on Wing Drag. T. N. No. 695, NACA, 1939.
13. Wood, Donald H.: Tests of Nacelle-Propeller Combinations in Various Positions with Reference to Wings. Part I. Thick Wing—N. A. C. A. Cowled Nacelle—Tractor Propeller. Rep. No. 415, NACA, 1932.
14. Stickle, George W.: Design of N. A. C. A. Cowlings for Radial Air-Cooled Engines. Rep. No. 662, NACA, 1939.

TABLE I.—NACELLE ORDINATES

[See fig. 6]

Nacelle nose ordinates (in.)			
Standard cowling		Streamline nose	
x	R'	x	R'
0	2.81	0.00	0.000
.05	3.00	.40	.726
.10	3.07	.75	1.093
.15	3.13	1.45	1.645
.20	3.18	2.85	2.354
.30	3.26	5.65	3.107
.40	3.32	8.45	3.430
.50	3.36	10.92	3.500
.60	3.39	----------	----------
.80	3.45	----------	----------
1.00	3.48	----------	----------
1.25	3.50	----------	----------
3.75	3.50	----------	----------

Nacelle afterbody ordinates (in.)						
	High position		Normal position		Low position	
x	R_U	R_L	R_U	R_L	R_U	R_L
0	3.50	3.50	3.50	3.50	3.50	3.50
2	3.48	3.48	3.48	3.48	3.48	3.48
4	3.30	------	3.30	3.30	3.46	3.30
6	2.99	------	2.99	3.12	3.43	3.02
8	2.56	------	2.56	2.89	--------	2.60
10	2.04	------	2.04	2.57	--------	2.08
12	1.41	------	1.41	2.24	--------	1.47
13.53	.97	------	------	------	--------	--------
14	------	------	------	1.88	--------	.82
16	------	------	------	--------	--------	.11
16.28	0	------	------	--------	--------	--------

TABLE II.—DRAG OF COMPONENT PARTS OF AIRPLANE MODEL

[Percentage of total drag coefficient at $M=0.20$]

PART	$\alpha=0°$ ($C_L=0.2$ approximately)				$\alpha=-2°$ ($C_L=0$ approximately)			
	Natural transition		Fixed transition		Natural transition		Fixed transition	
	$M=0.20$	$M=0.57$	$M=0.20$	$M=0.57$	$M=0.20$	$M=0.57$	$M=0.20$	$M=0.57$
	Standard model							
Wing	36	37	41	42	35	34	38	38
Fuselage and fillet	26	27	24	25	24	27	23	25
Nacelles ($K=0.08$, $\frac{\Delta p}{q}=0.80$)	18	18	15	15	18	19	16	19
Tail group	9	9	10	9	12	12	12	12
Main wheels	9	12	8	12	9	11	9	11
Tail wheel	2	3	2	2	2	3	2	3
Total C_D	100	106	100	105	100	106	100	108
	Improved model							
Wing	48	49	51	52	47	45	48	49
Fuselage and fillet	29	28	25	25	28	29	26	26
Tail group	12	11	12	10	15	14	15	14
Nacelles	5	5	7	5	5	5	6	6
Cooling drag (estimated)	6	2	5	2	5	2	5	2
Total C_D	100	95	100	94	100	95	100	97

U. S. GOVERNMENT PRINTING OFFICE: 1945

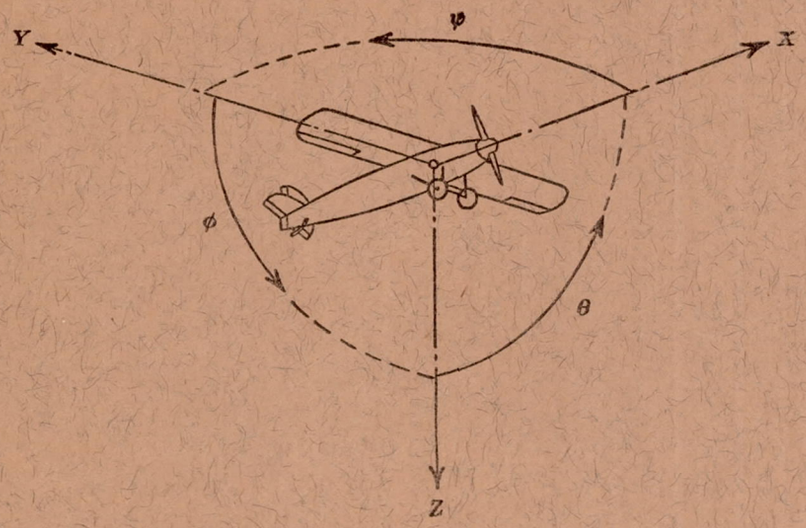

Positive directions of axes and angles (forces and moments) are shown by arrows

Axis		Force (parallel to axis) symbol	Moment about axis			Angle		Velocities	
Designation	Symbol		Designation	Symbol	Positive direction	Designation	Symbol	Linear (component along axis)	Angular
Longitudinal	X	X	Rolling	L	$Y \longrightarrow Z$	Roll	φ	u	p
Lateral	Y	Y	Pitching	M	$Z \longrightarrow X$	Pitch	θ	v	q
Normal	Z	Z	Yawing	N	$X \longrightarrow Y$	Yaw	ψ	w	r

Absolute coefficients of moment

$C_l = \frac{L}{qbS}$ (rolling) $\quad C_m = \frac{M}{qcS}$ (pitching) $\quad C_n = \frac{N}{qbS}$ (yawing)

Angle of set of control surface (relative to neutra position), δ. (Indicate surface by proper subscript.)

4. PROPELLER SYMBOLS

D Diameter

p Geometric pitch

p/D Pitch ratio

V' Inflow velocity

V_s Slipstream velocity

T Thrust, absolute coefficient $C_T = \frac{T}{\rho n^2 D^4}$

Q Torque, absolute coefficient $C_Q = \frac{Q}{\rho n^2 D^5}$

P Power, absolute coefficient $C_P = \frac{P}{\rho n^3 D^5}$

C_s Speed-power coefficient $= \sqrt[5]{\frac{\rho V^5}{P n^2}}$

η Efficiency

n Revolutions per second, rps

Φ Effective helix angle $= \tan^{-1}\left(\frac{V}{2\pi r n}\right)$

5. NUMERICAL RELATIONS

1 hp=76.04 kg-m/s=550 ft-lb/sec

1 metric horsepower=0.9863 hp

1 mph=0.4470 mps

1 mps=2.2369 mph

1 lb=0.4536 kg

1 kg=2.2046 lb

1 mi=1,609.35 m=5,280 ft

1 m=3.2808 ft